NASA/TM—2016-219098

Characterization of Three-Stream Jet Flow Fields

Brenda S. Henderson and Mark P. Wernet
Glenn Research Center, Cleveland, Ohio

July 2016

NASA STI Program . . . in Profile

Since its founding, NASA has been dedicated to the advancement of aeronautics and space science. The NASA Scientific and Technical Information (STI) Program plays a key part in helping NASA maintain this important role.

The NASA STI Program operates under the auspices of the Agency Chief Information Officer. It collects, organizes, provides for archiving, and disseminates NASA's STI. The NASA STI Program provides access to the NASA Technical Report Server—Registered (NTRS Reg) and NASA Technical Report Server—Public (NTRS) thus providing one of the largest collections of aeronautical and space science STI in the world. Results are published in both non-NASA channels and by NASA in the NASA STI Report Series, which includes the following report types:

- TECHNICAL PUBLICATION. Reports of completed research or a major significant phase of research that present the results of NASA programs and include extensive data or theoretical analysis. Includes compilations of significant scientific and technical data and information deemed to be of continuing reference value. NASA counter-part of peer-reviewed formal professional papers, but has less stringent limitations on manuscript length and extent of graphic presentations.

- TECHNICAL MEMORANDUM. Scientific and technical findings that are preliminary or of specialized interest, e.g., "quick-release" reports, working papers, and bibliographies that contain minimal annotation. Does not contain extensive analysis.

- CONTRACTOR REPORT. Scientific and technical findings by NASA-sponsored contractors and grantees.

- CONFERENCE PUBLICATION. Collected papers from scientific and technical conferences, symposia, seminars, or other meetings sponsored or co-sponsored by NASA.

- SPECIAL PUBLICATION. Scientific, technical, or historical information from NASA programs, projects, and missions, often concerned with subjects having substantial public interest.

- TECHNICAL TRANSLATION. English-language translations of foreign scientific and technical material pertinent to NASA's mission.

For more information about the NASA STI program, see the following:

- Access the NASA STI program home page at http://www.sti.nasa.gov

- E-mail your question to help@sti.nasa.gov

- Fax your question to the NASA STI Information Desk at 757-864-6500

- Telephone the NASA STI Information Desk at 757-864-9658

- Write to:
  NASA STI Program
  Mail Stop 148
  NASA Langley Research Center
  Hampton, VA 23681-2199

NASA/TM—2016-219098

Characterization of Three-Stream Jet Flow Fields

Brenda S. Henderson and Mark P. Wernet
Glenn Research Center, Cleveland, Ohio

National Aeronautics and
Space Administration

Glenn Research Center
Cleveland, Ohio 44135

July 2016

Acknowledgments

The Commercial Supersonics Technology Project of the Advanced Air Vehicles Program at NASA supported this work.

Level of Review: This material has been technically reviewed by technical management.

Available from

NASA STI Program
Mail Stop 148
NASA Langley Research Center
Hampton, VA 23681-2199

National Technical Information Service
5285 Port Royal Road
Springfield, VA 22161
703-605-6000

This report is available in electronic form at http://www.sti.nasa.gov/ and http://ntrs.nasa.gov/

Characterization of Three-Stream Jet Flow Fields

Brenda S. Henderson and Mark P. Wernet
National Aeronautics and Space Administration
Glenn Research Center
Cleveland, Ohio 44135

Abstract

Flow-field measurements were conducted on single-, dual- and three-stream jets using two-component and stereo Particle Image Velocimetry (PIV). The flow-field measurements complimented previous acoustic measurements. The exhaust system consisted of externally-plugged, externally-mixed, convergent nozzles. The study used bypass-to-core area ratios equal to 1.0 and 2.5 and tertiary-to-core area ratios equal to 0.6 and 1.0. Axisymmetric and offset tertiary nozzles were investigated for heated and unheated high-subsonic conditions. Centerline velocity decay rates for the single-, dual- and three-stream axisymmetric jets compared well when axial distance was normalized by an equivalent diameter based on the nozzle system total exit area. The tertiary stream had a greater impact on the mean axial velocity for the small bypass-to-core area ratio nozzles than for large bypass-to-core area ratio nozzles. Normalized turbulence intensities were similar for the single-, dual-, and three-stream unheated jets due to the small difference (10 percent) in the core and bypass velocities for the dual-stream jets and the low tertiary velocity (50 percent of the core stream) for the three-stream jets. For heated jet conditions where the bypass velocity was 65 percent of the core velocity, additional regions of high turbulence intensity occurred near the plug tip which were not present for the unheated jets. Offsetting the tertiary stream moved the peak turbulence intensity levels upstream relative to those for all axisymmetric jets investigated.

I. Introduction

Future turbine-engine architectures for supersonic commercial aircraft may provide a third exhaust stream that will be available for potential noise-reduction technologies. A third jet stream allows for additional geometric and parametric variation of the nozzle operation, and for an offset of the third stream relative to the core and bypass streams. The introduction of asymmetry into the flow field of the jet provides the potential for re-directing noise away from certain observer locations. Recent experimental investigations (Refs. 1 and 2) have focused on quantifying the noise radiation for a range of axisymmetric and offset three-stream jet configurations for subsonic and supersonic exhausts to identify viable technologies for future supersonic aircraft and to form a database for noise prediction codes. These studies (Ref. 2) have also investigated the potential of Reynolds-Averaged Navier-Stokes based acoustic analogies to capture the azimuthal variation inherent in the sound field produced by offset configurations. An accompanying effort (Ref. 3) investigates the ability of three-stream technologies to meet future FAA noise requirements for NASA's N+2 Supersonic Aircraft. The present study focusses on the flow-field characteristics of high subsonic heated and unheated three-stream jets. The intent of the study is to compare the mean and turbulent characteristics of the various axisymmetric and offset configurations investigated in previous acoustic studies.

Early acoustic investigations with three-stream jets (Ref. 4) focused on using the third velocity field to reduce the shearing rate at the outer flow boundary and to modify the jet shock structure in inverted-velocity-profile supersonic jets. More recent three-stream experiments with high speed jets (Ref. 5) showed axisymmetric configurations provided no acoustic benefit over single-stream jets for very low (less than 0.2) bypass-to-core area ratio nozzles. In these very low bypass-ratio nozzles, offset tertiary streams provided significant noise reduction (up to 5 dB overall) on the "thick side" of the jet relative to

that for a coaxial nozzle system. Recent experiments (Ref. 2) with moderate (between 1 and 3) bypass-to-core area ratio nozzles showed noise reduction associated with the addition of a tertiary stream to a high subsonic dual-stream jet depended on the area ratios of the nozzles and on the tertiary stream operating condition. Larger noise reductions (relative to the dual-stream jet) were achieved with an offset tertiary stream than with the axisymmetric configurations, although the noise reduction benefit of the offset stream diminished as the jet velocities of the core and bypass streams decreased.

Early investigations (Ref. 6) into the flow characteristics of single-stream jets documented the mean flow development and turbulence characteristics for 0.2 to 0.7 Mach number jets. Witze (Ref. 7) developed an expression for the centerline velocity decay which accounted for jet density and provided good agreement with a significant number of existing experimental results. Early research into the flow characteristics of free-shear layers, summarized by Birch and Eggers (Ref. 8), focused on velocity decay rates and jet spreading characteristics. An in-depth investigation of subsonic and supersonic single-stream jets (Ref. 9) documented mean velocity and turbulent characteristics and associated scaling approaches for collapsing data throughout the jet plumes. Recent efforts have looked at the development of a consensus dataset of turbulent statistics for hot subsonic jets (Ref. 10). Yoder, DeBonis, and Georgiadis (Ref. 11) provide a reasonably comprehensive review of experimental and numerical results for free shear layers including single-stream jets.

One of the first investigations into the flow characteristics of multistream jets focused on co-flow jets (a single-stream jet in a wind tunnel) and showed that the jet spreading rate was governed by the velocity ratio of the two flow streams. More recent investigations have looked at the mean and turbulent characteristics of jets exhausting from externally mixed, externally plugged dual-stream nozzles with bypass ratios roughly equal to five (Refs. 12 and 13). The turbulence characteristics associated with these coaxial jets displayed asymmetries that have been explained by Birch et al. (Ref. 14) as being associated with a basic instability of the jet configuration. Mean flow characteristics of high-speed (Mach 1.5) eccentric dual-stream jets were documented by Murakami and Papamoschou (Ref. 15) and compared with single-stream and axisymmetric dual-stream jets for bypass-to-core area ratios in the range of 0.9 to 3.0. These investigations used coplanar nozzles. Little or no flow-field data is available for multistream jets with bypass-to-core nozzle-exit areas in the range of those investigated here using noncoplanar nozzles with external plugs.

The present investigation uses Particle Image Velocimetry (PIV) measurements to investigate the mean and turbulent characteristics of single-, dual-, and three-stream jets. The model system uses a set of externally mixed, externally plugged, convergent nozzles. Single- and dual-stream jets are produced by operating only the core and the core along with the bypass streams, respectively. The three-stream studies include axisymmetric and offset configurations. The analysis focuses on comparisons of axial mean velocity and axial turbulence intensity for the various configurations although it is recognized that additional flow-field quantities will need to be investigated for future noise prediction efforts. Mean axial vorticity is also included for the offset configuration. The experiments used heated and unheated high-subsonic exhaust conditions. The Experimental Approach is presented in Section II. Experimental results for the axial mean velocity and the axial component of the turbulence intensity are presented in Sections III A and B, respectively. Conclusions are found in Section IV.

II. Experimental Approach

The experiments were performed in the Aero-Acoustic Propulsion Laboratory (AAPL) at the NASA Glenn Research Center shown in Figure 1. The AAPL is a 20 m radius geodesic dome treated with acoustic wedges. The AAPL contains the Nozzle Acoustic Test Rig (NATR), which produces a 1.35 m diameter simulated forward flight stream reaching Mach numbers of 0.35 and contains the High Flow Jet Exit Rig (HFJER), a three-stream jet engine simulator capable of replicating most commercial turbo-fan engine temperatures and pressures (Ref. 16).

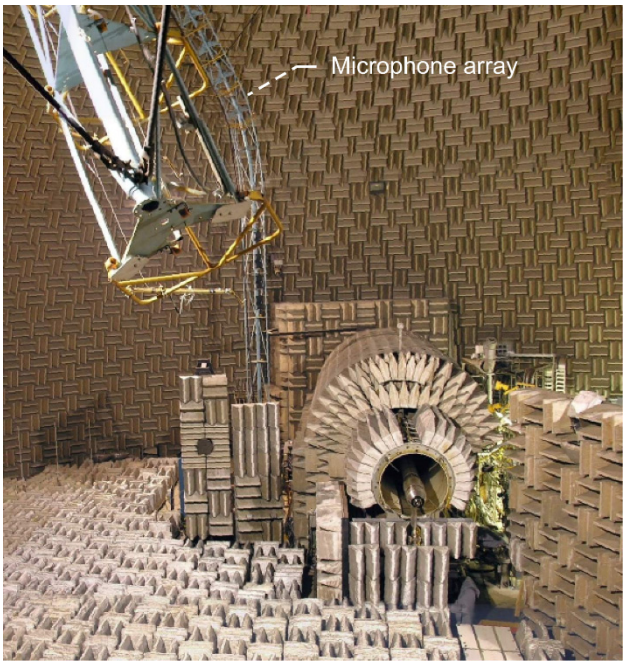

Figure 1.—A photograph of the Aero-Acoustic Propulsion Laboratory (AAPL) showing the Nozzle Acoustic Test Rig (NATR) and the High Flow Jet Exit Rig (HFJER).

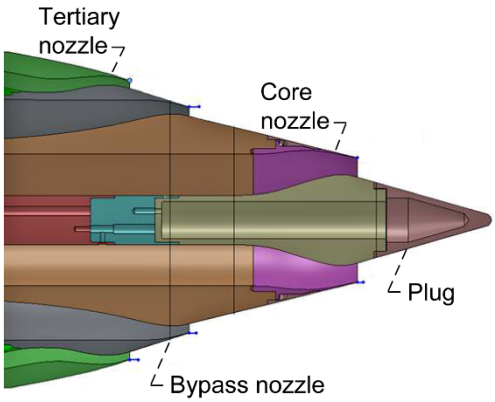

Figure 2.—The axisymmetric-nozzle system used in the three-stream experiments.

The flow-field experiments used an externally-mixed, externally-plugged, convergent nozzle system with the tertiary-to-core-area ratios (A_t/A_c) equal to 1.0 and 0.6 and bypass-to-core-area ratios (A_b/A_c) equal to 2.5 and 1.0. An axisymmetric configuration is shown in Figure 2. All configurations used a core-nozzle exit diameter and area of 13.2 and 69.7 cm^2, respectively, and a common bypass nozzle. The bypass-to-core-area ratio was varied by using core nozzles with slightly different external contours which resulted in differences in the bypass-nozzle exit area. Tertiary nozzles with slightly different internal contours and exit areas were used to vary the tertiary-to-core area ratio. The single- and dual-stream configurations used the three-stream nozzle system with no flow through the bypass and tertiary streams for the single-stream experiments and no flow through the tertiary stream for the dual-stream experiments.

Tertiary-stream offset was achieved with the introduction of an offset duct upstream of the tertiary nozzle (Fig. 3). The offset duct, which was combined with the $A_t/A_c = 1.0$ tertiary nozzle, produced a 0.156 in. offset of the tertiary nozzle centerline relative to the centerlines of the core and bypass nozzles.

The flow conditions used in the experiments are shown in Table 1. Additional supersonic conditions were used in previous acoustic studies (Ref. 1). The nozzle pressure ratio, NPR, is the ratio of the stagnation pressure of the jet to the ambient pressure. The nozzle temperature ratio, NTR, is the ratio of the stagnation temperature of the jet to the ambient temperature. Subscripts c, b, and t refer to the core, bypass, and tertiary streams, respectively. For heated core-stream conditions, $NTR_b = NTR_t = 1.25$. For the unheated conditions in Table 1, the temperature of the multiple jet streams was roughly 360 K as this temperature provided optimum PIV results. The experiments were conducted at simulated forward flight Mach numbers (M_{fj}) of 0.0 and 0.3.

Particle Image Velocimetry (PIV) studies included two-component measurements in a streamwise plane, with the light sheet oriented along the centerline of the jet, and stereo PIV measurements, with a cross-stream orientation of the light sheet. The two-component measurements provided vector maps for up to 14 exit core diameters downstream of the plug tip. Stereo PIV measurements acquired data for one half of the jet and axial locations up to nine exit-core diameters downstream of the plug tip.

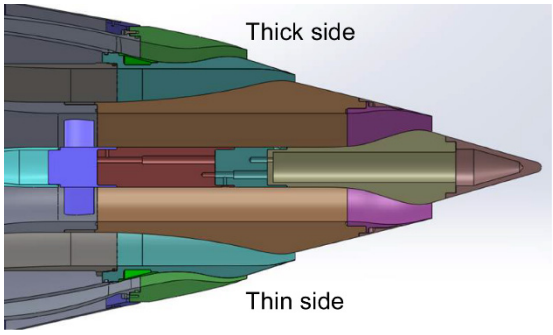

Figure 3.—The offset nozzle system used in the three-stream experiments.

TABLE 1.—FLOW CONDITIONS

Experiment	NPR_c	NPR_b	NPR_t	Jet Type
Unheated	1.8	1.0	1.0	Single
		1.6	1.0	Dual
			1.2, 1.8	Three
Heated, NTR_c = 3.0	1.8	1.0	1.0	Single
		1.8	1.0	Dual
			1.4 - 2.1	Three

The stereo PIV system was configured to provide cross-stream measurements of the three-component velocity field. The PIV system was mounted on a large traverse system. The entire cross-stream flow field could not be captured with sufficient spatial resolution to meet the test requirements. Hence, only the one half of the flow field was acquired. The Stereo PIV system employed two high-resolution (4008×2672 pixels) cameras, mounted in landscape mode, equipped with 180 mm focal length lenses and 8 mm extension tubes to provide a 526×272 mm (W×H) field of view. The PIV system was positioned so that the top edge of the field of view was approximately 25 mm above the nozzle centerline. The cameras were mounted downstream of the model exit plane at nominally ±45° from the nozzle centerline. Stereo PIV calibrations were performed using a single plane target translated to 9 axial positions over a ±2 mm range. A 4th-order polynomial was used in the calibration and a calibration verification operation was employed to ensure the calibration overlapped the laser light sheet plane. The measurement plane was illuminated with a dual head 400 mJ/pulse Nd:YAG laser system. The laser beams were formed into 1 by 550 mm light sheets using cylindrical and spherical lenses. Both cameras were connected to a single computer system via a CameraLink PCI card and the 400 frame pair data sequences were acquired and streamed to disk at a rate of 2 frame-pairs/camera/sec.

In order to facilitate a large field of view and high spatial resolution in the two-component PIV measurements, a four camera, 2×2 configuration was used. The 4008×2672 pixel stereo PIV cameras were used with their 4008-pixel axis oriented vertically (portrait mode). The cameras were equipped with 180 mm focal length lenses and positioned so that their fields of view overlapped by 2.54 cm. A PIV calibration target was used to calibrate and register all four cameras. The physical registration of the four cameras was used in the setup of the vector processing grids in the top-left, top-right and bottom-left and bottom-right camera images so that no interpolation was required in the merging of the left/right vector maps. The final merged camera vector map covered an area of 355×560 mm (W×H). All four cameras were connected to a single computer system via two CameraLink PCI cards and the 400 frame pair data sequences were acquired and streamed to disk at a rate of two frame-pairs/camera/sec.

Four independent seeding systems were required in this study: core stream, bypass stream, tertiary stream and ambient flow. The heated core and bypass streams were seeded with 0.5 μm diameter alumina powder. A dispersion of the alumina seed material in ethanol was prepared using a pH stabilization technique (Ref. 17). The alumina/ethanol was dispersed in the flow well upstream of the nozzle using an air-assisted atomizing nozzle. The pH stabilization technique provides highly dispersed, unagglomerated seed particles in the flow. The tertiary stream was also seeded using the pH stabilized aluminum oxide dispersion. The ambient free-jet flow was seeded using a propylene glycol liquid seed material. Several fog generators were setup in the inlet tunnel to the free-jet—allowing nearly 18 m of mixing before entering the PIV measurement planes.

The PIV image data were processed using multipass correlation with 64×64 pixel subregions on 32 pixel centers, followed by 32×32 pixel subregions on 16 pixels centers. Subregion distortion processing was also used to process the PIV data (Ref. 18). Subregion distortion was used to correct for velocity gradients across the subregion and to minimize the “peak-locking” effect, which is the tendency

for the estimated particle displacements to preferentially concentrate at integer values. In the subregion distortion technique, the local velocity gradients surrounding the current correlation subregion are used to distort the subregion before the cross-correlation processing operation. Distorting the subregion yields correlation subregions with uniform particle displacements, and hence, reduces any bias caused by the velocity gradients. Typically two additional passes after the multipass processing are used with subregion distortion applied to refine the correlation peak estimates. Due to the oblique viewing of the model in the stereo PIV configuration, the nozzle was recorded in both the left and right camera views. The image of the nozzle corrupts the background in the image—leading to a loss of correlation in regions where the model is brightly illuminated by the laser light sheet. The Symmetric Phase Only Filtering (SPOF) technique was also applied in the data processing to mitigate any effects from the model being in the background of the images near the exit plane (Ref. 19). The final cross-stream velocity vector maps had 2 mm spatial resolution. The final 2-D streamwise velocity vector maps had a spatial resolution of 1.5 mm. Sequences of 400 velocity vector maps were acquired at each measurement station and ensemble averaged to provide first and second order statistics over the entire measurement plane. Chauvenet's criteria was used to eliminate any outliers in the ensemble averaging process (Ref. 20).

III. Experimental Results

A. Mean Axial Velocity

Mean velocity contour plots obtained with the two-component PIV system for the unheated and heated single-stream jets and $A_b/A_c = 1$ are shown in Figure 4. The mean axial velocity, U, and streamwise and radial coordinates (x and y) have been normalized by the jet exit velocity, U_e, and the equivalent core diameter based on the core-nozzle exit area, D_{eqc}, respectively. The origin of the streamwise coordinate, x, is the plug tip. For externally plugged nozzles, the flow exits the nozzle at an angle to the jet axis and reorients toward the axis with downstream distance. A shear layer develops along the periphery of the jet and a boundary layer grows along the plug. At the plug tip, a wake forms. As shown in the Figure, the plug wake persists further downstream for the unheated jet than for the heated jet and the potential core for the heated jet is shorter than that for the unheated jet.

The mean velocity in cross-stream planes for the unheated single-stream jet are shown in Figure 5. The mean velocity has been normalized by the maximum centerline velocity, U_{cl}. For $0 \leq x/D_{eqc} \leq 5$, the peak velocity occurs outboard of the jet centerline. As the axial distance increases from the plug tip, the maximum and centerline velocities first increase and then decrease.

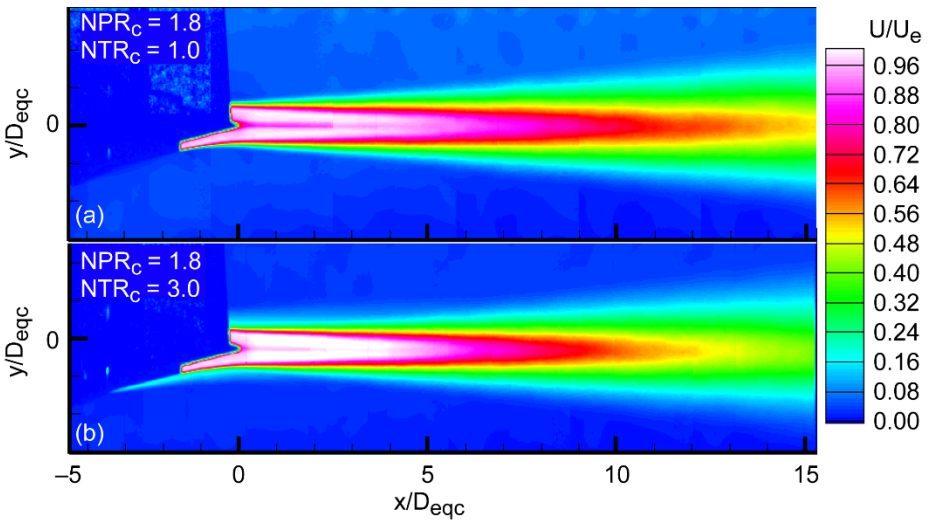

Figure 4.—The velocity in the center plane for the unheated and heated single-stream jets. The data were acquired at $M_{fj} = 0.0$.

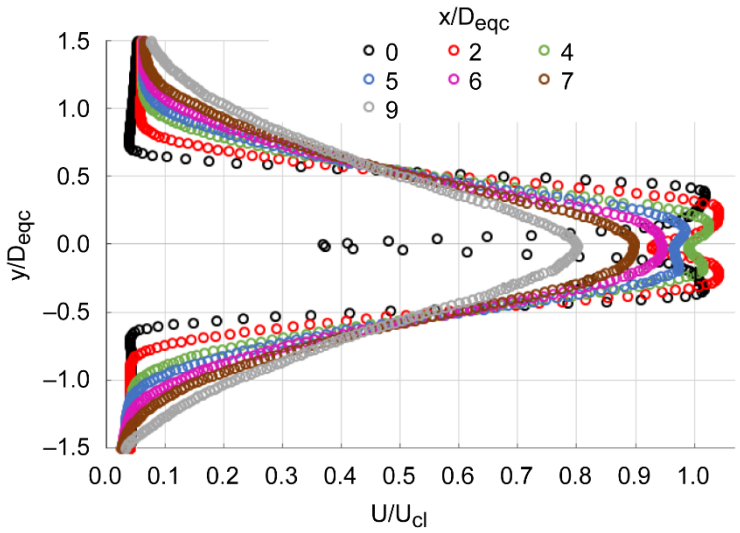

Figure 5.—The velocity at the indicated cross-stream planes for the simulated single-stream unheated jet.

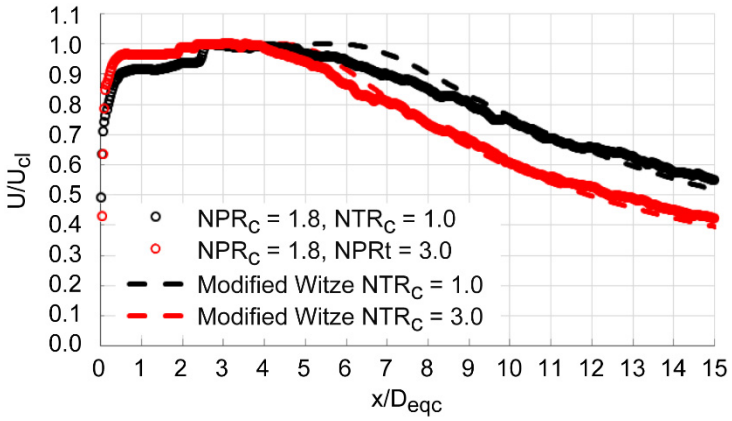

Figure 6.—The centerline velocity normalized by the peak centerline velocity for the simulated single-stream jets. The PIV data are indicated with circles. Predicted centerline velocities based on Witze (Ref. 7) are indicated by dashed lines.

The mean centerline velocities for the hot and cold single-stream jets are shown in Figure 6. The data have been smoothed by averaging in the axial direction over three PIV data points. The centerline velocities predicted by a modified Witze (Ref. 7) equation are indicated by dashed lines in the Figure. The nondimensional correlation parameter core length, X_c, in Witze's equation has been changed from 0.7 to 0.65. The jets used in this study are different from those used in Reference 7 as the plug wake introduces a shear layer in center of the jet that impacts the jet mixing characteristics. Additionally, the jet shear layer begins at the exit of the core nozzle, well upstream of the plug tip, and, therefore, will be thicker at the axial location of the plug tip than the initial shear layers for the jets considered by Witze. The decay rates of the measured and predicted centerline velocities are similar. The predicted potential core lengths are slightly greater than those measured. The prediction for the heated jet is slightly better than that for the unheated jet likely due to the plug wake mixing faster for the heated jet than the unheated jet. It should be noted that the change in centerline velocity with downstream distance may not be a true indication of potential-core length as the peak velocity occurs outboard of the centerline. However, it will be shown that the centerline velocity decay roughly mimics the decay of the peak velocity once the centerline velocity has reached a maximum.

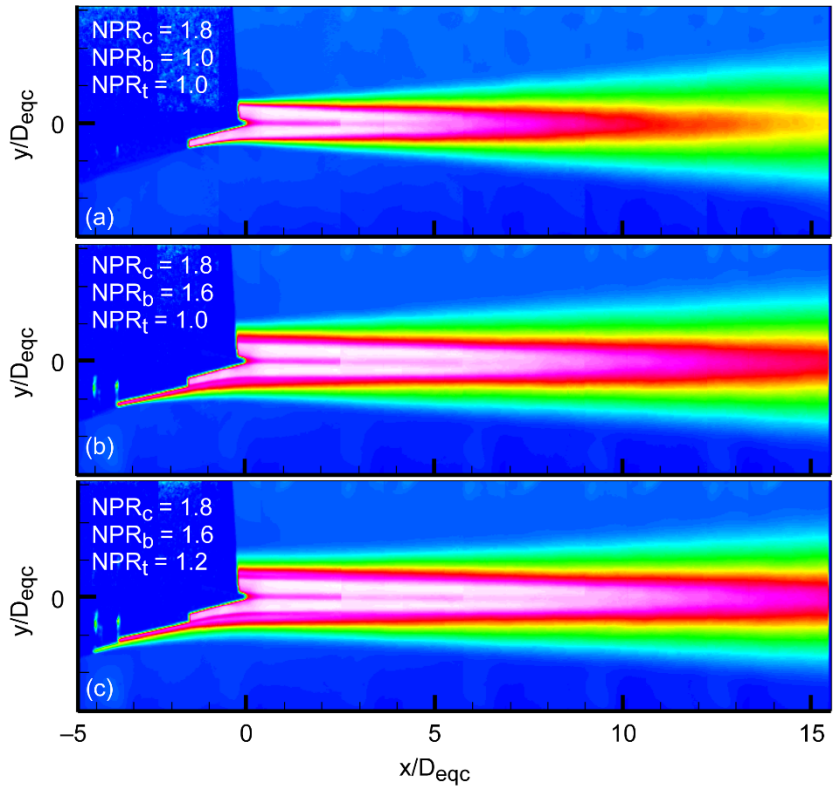

Figure 7.—The velocities in the center plane for the unheated single-, dual-, and three-stream jets. The conditions are indicated on the contour plots. The legend is the same as that in Figure 4 with U_e equal to the core exit velocity. The data were acquired for M_{fj} = 0.0.

Contour plots of the mean velocities for the single-, dual-, and three-stream jets at unheated conditions are shown in Figure 7 for $A_b/A_c = A_t/A_c = 1.0$. The addition of the bypass stream to the single-stream jet increases the potential-core length and an additional slight increase in potential-core length is achieved with the further addition of the tertiary stream.

The centerline axial velocities for the conditions in Figure 7 are shown in Figure 8. The streamwise distance from the nozzle tip, normalized by the equivalent diameter computed from the nozzle-system total exit area, x/D_{eqA}, has been used for the abscissa in Figure 8(b). For the dual-stream jet, the bypass-stream exit velocity is 90 percent of the core-stream exit velocity. For the three-stream jet, the tertiary-stream exit velocity is 63 percent of the bypass-stream exit velocity. As shown in Figure 8(a), adding an annular jet stream increases the potential core length and reduces the centerline velocity decay rate. A reasonable collapse of the centerline velocity data is obtained when the axial distance is normalized by D_{eqA} (Fig. 8(b)). Also shown by the green data in Figure 8(b) are the peak axial velocities in the cross-stream planes. The peak velocity has been normalized by the jet exit velocity. The normalized peak and centerline velocities show similar decay rates and, therefore, may be used interchangeably when computing potential-core length.

The centerline velocities for the single- and three-stream heated jets with $M_{fj} = 0.0$ are shown in Figure 9. The data are for $A_b/A_c = A_t/A_c = 1$. For the three-stream jet, the bypass-stream exit velocity is 65 percent of the core-stream exit velocity and the tertiary-stream exit velocity is 76 percent of the bypass-stream exit velocity. Similar to the unheated conditions, the centerline decay rates downstream of the potential core are the same for the single and three-stream jets. However, the potential-core length for the single-stream jet is slightly longer than that for the three-stream jet. The data for the two jet

configurations overlap if the three-stream data are moved downstream by $0.5D_{eqA}$, an indication that it may be necessary to adjust the origin when comparing data from multistream jets, and the adjustment is likely dependent on the bypass-to-core velocity ratio (as it will be shown subsequently that the tertiary-stream conditions do not impact the normalized potential-core length).

The data for heated three-stream jets with $A_b/A_c = A_t/A_c = 1$ are compared in Figure 10 for static and $M_{fj} = 0.3$ simulated flight-stream conditions. The results show the introduction of the simulated forward-flight stream has little impact on the velocity decay rate downstream of the potential core and slightly increases the potential-core length.

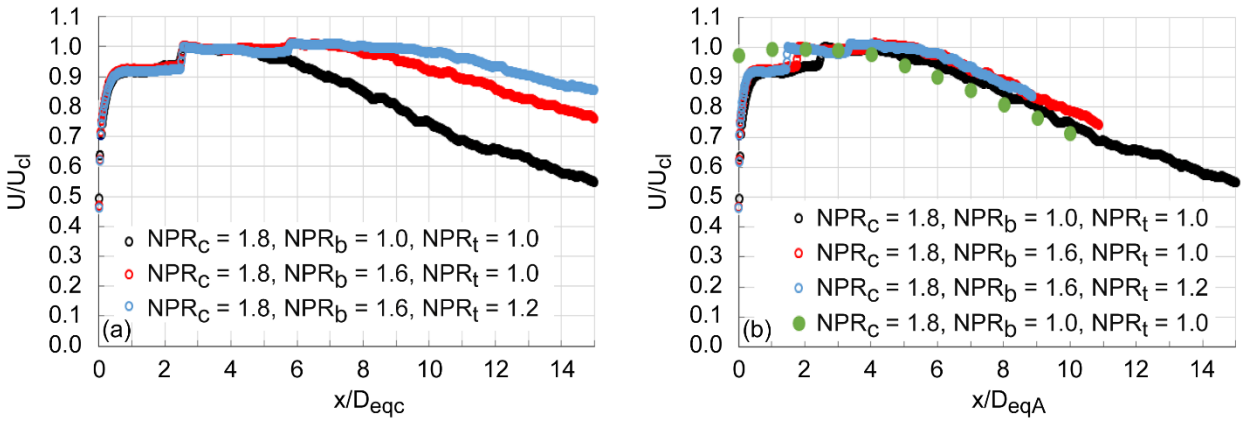

Figure 8.—The centerline velocities for the unheated jets at the indicated nozzle pressure ratios. The abscissa has been normalized by the equivalent core diameter in (a) and the equivalent diameter based on total nozzle-system exit area in (b). The data indicated by green circles in (b) are for the peak jet velocity in the indicated cross-stream plane. The peak velocity has been normalized by the jet exit velocity. The data were acquired for $M_{fj} = 0.0$.

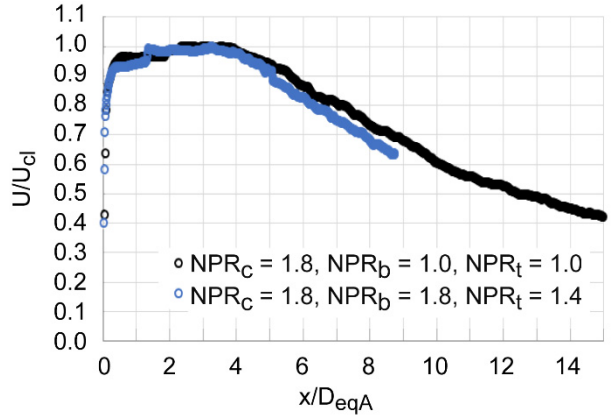

Figure 9.—The centerline velocities at the indicated nozzle pressure ratios and $NTR_c = 3.0$. The data were acquired for $M_{fj} = 0.0$.

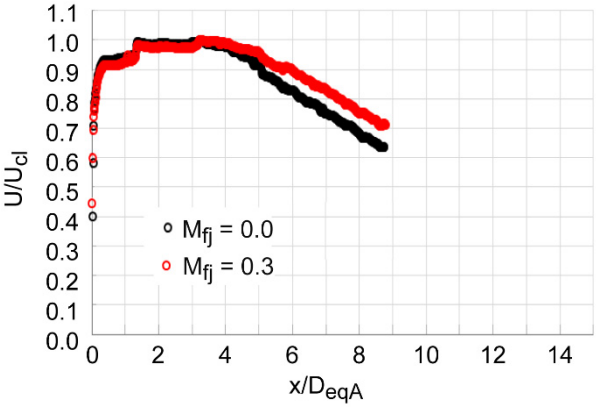

Figure 10.—The centerline velocities for NPRc = NPRb = 1.8, NPRt = 1.4, NTRc = 3.0 and the indicated free jet Mach numbers.

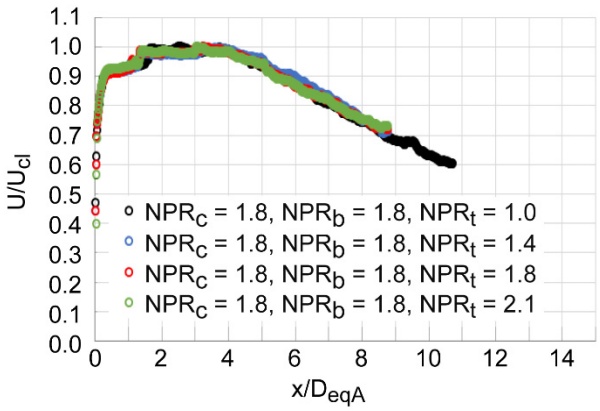

Figure 11.—The centerline velocities for the indicated nozzle pressure ratios and NTR_c = 3.0. The data were acquired for $A_b/A_c = A_t/A_c$ = 1.0 and M_{fj} = 0.3.

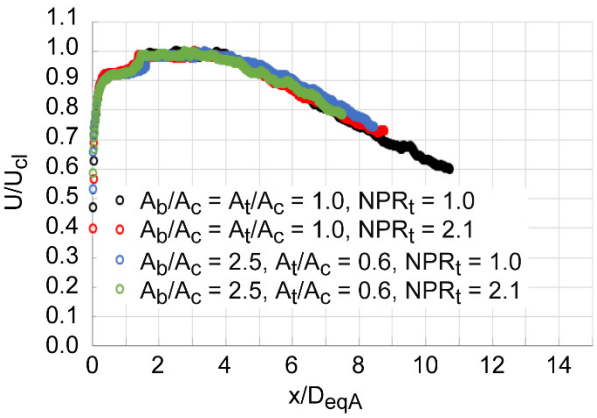

Figure 12.—The centerline velocities for $NPR_c = NPR_b$ = 1.8, NTR_c = 3.0, and the indicated area ratios and NPR_t. The data were acquired for M_{fj} = 0.3.

The impact of NPR_t on centerline velocity for the heated jet conditions and M_{fj} = 0.3 is shown in Figure 11 for $A_b/A_c = A_t/A_c$ = 1.0. Increasing NPR_t from 1.4 to 2.1 is shown to have no impact on the potential core length and velocity decay rate when data are compared at the same normalized axial coordinate. Data acquired for other bypass-to-core and tertiary-to-core area ratios produced similar results.

The centerline velocities for heated dual- and three-stream jets produced by two nozzle systems with different bypass-to-core and tertiary-to-core area ratios are shown in Figure 12. Data for NPR_t = 1.0 (dual stream) and NPR_t = 2.1 are shown in the Figure. The data indicate that scaling the axial distance by the D_{eqA} collapses the centerline axial-velocity data for all bypass-to-core and tertiary-to-core area ratios investigated. Data acquired with the A_b/A_c = 1.0 and A_t/A_c = 0.6 nozzle system produced similar results to those shown in Figure 12.

The velocities in cross-stream planes for the unheated and heated single-stream jets are shown in Figures 13 and 14, respectively. The data have not been axially averaged. The velocities have been normalized by the peak velocity, U_p, at each axial station and the cross-stream coordinate, y, has been normalized by $r_{1/2}$ (used to determine jet spreading rate), the radial distance to the location of $U_p/2$. For the unheated jet, the effects of the plug on the central region of the jet are observed in the velocity data at axial stations up to, and including x/D_{eqA} = 5. The self similar region occurs at roughly x/D_{eqA} = 6. For the heated jet, the effect of the plug is nearly imperceptible for x/D_{eqA} = 5 and the self-similar region of the jet occurs between 5 and 6 equivalent diameters. The velocity as a function of $(y-y_{1/2})/x$, where $y_{1/2}$ is the radial position to the location where $U = U_e/2$, is shown in Figure 15 for the unheated jet. The velocity profiles in Figure 15 are similar to those for a single stream jet with no external plug (Ref. 9). For $x/D_{eqA} \geq 3$ in the cross-plane region where $(y-y_{1/2})/x$ is a linear function of U/U_e, the normalize velocity profiles at the various cross-stream planes overlap. Similar trends to those in Figure 15 were obtained for the heated jet.

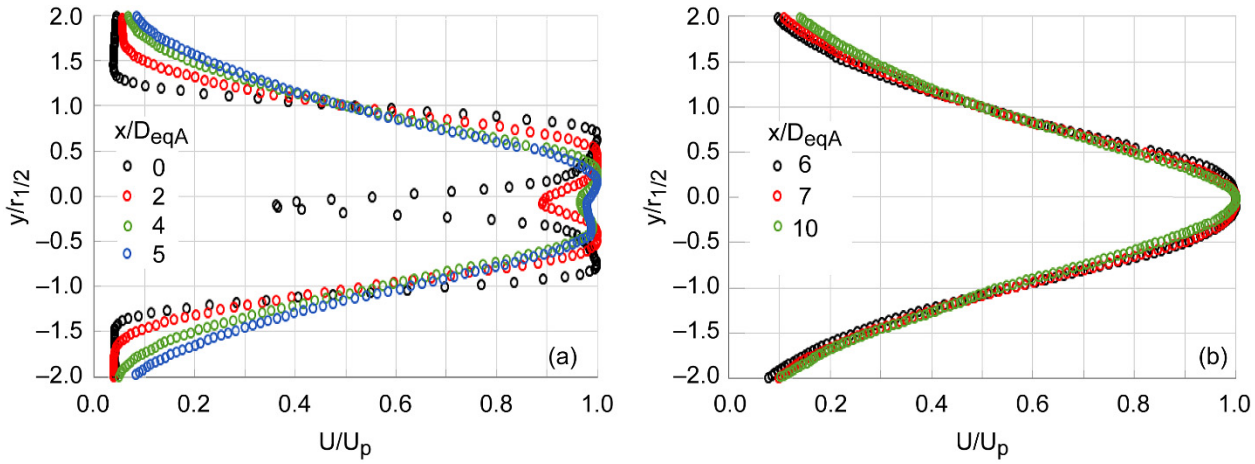

Figure 13.—The velocity at the indicated cross-stream planes for the unheated single-stream jet and M_{fj} = 0.0.

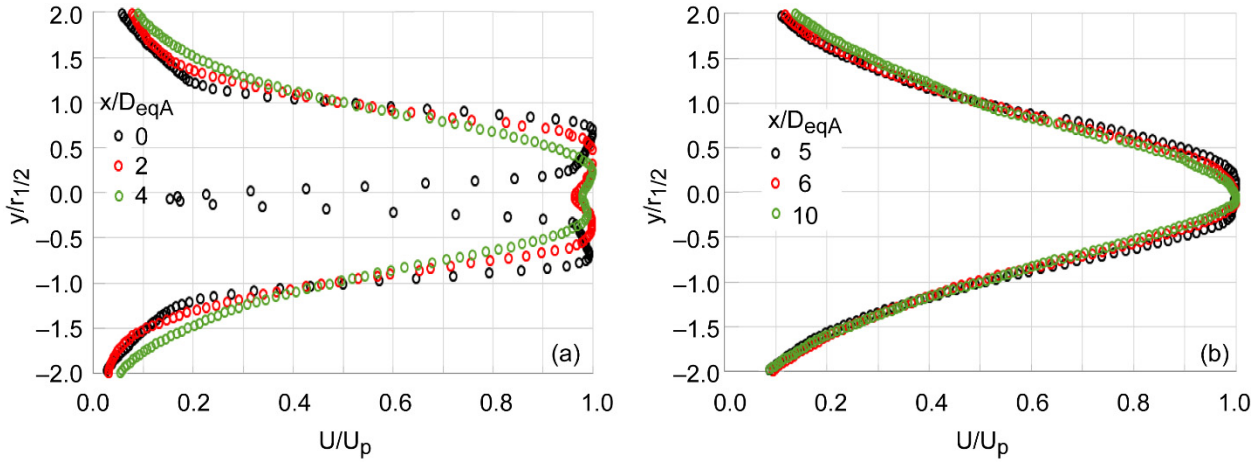

Figure 14.—The velocity at the indicated cross-stream planes for the heated single-stream jet and M_{fj} = 0.0.

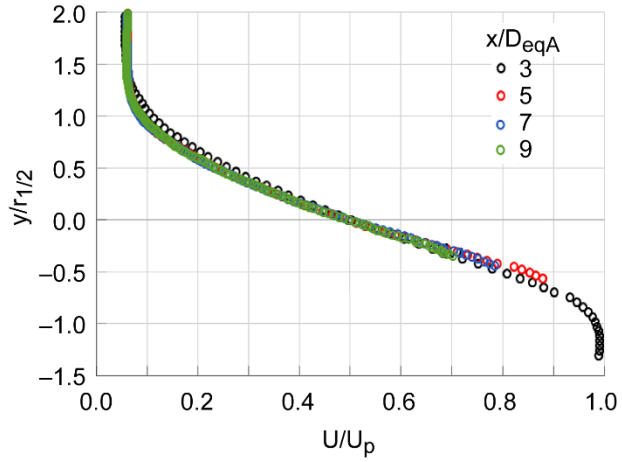

Figure 15.—The velocity at the indicated cross-stream planes for the unheated single-stream jet and M_{fj} = 0.0.

The velocities in cross-stream planes for the single-stream (S) and dual-stream (D) jets and for the single-stream and three-stream (T) jets are shown in Figures 16 and 17, respectively. The data are for unheated conditions, $A_b/A_c = A_t/A_c = 1.0$, and $M_{fj} = 0.0$. Near the plug tip ($x/D_{eqA} = 0$), the addition of the bypass flow produces a step change in the velocity profile at roughly $y/r_{1/2} = \pm 0.75$ (Fig. 16) which is still evident in the data at $x/D_{eqA} = 2$. For the three-stream jet, there is evidence of the bypass potential core at $x/D_{eqA} = 0$. The normalized velocity profiles for the single-, dual-, and three-stream jets are nearly identical by $x/D_{eqA} = 4$ and the self-similar regions of the jets are reached for all conditions in Figures 16 and 17 by roughly $x/D_{eqA} = 6$.

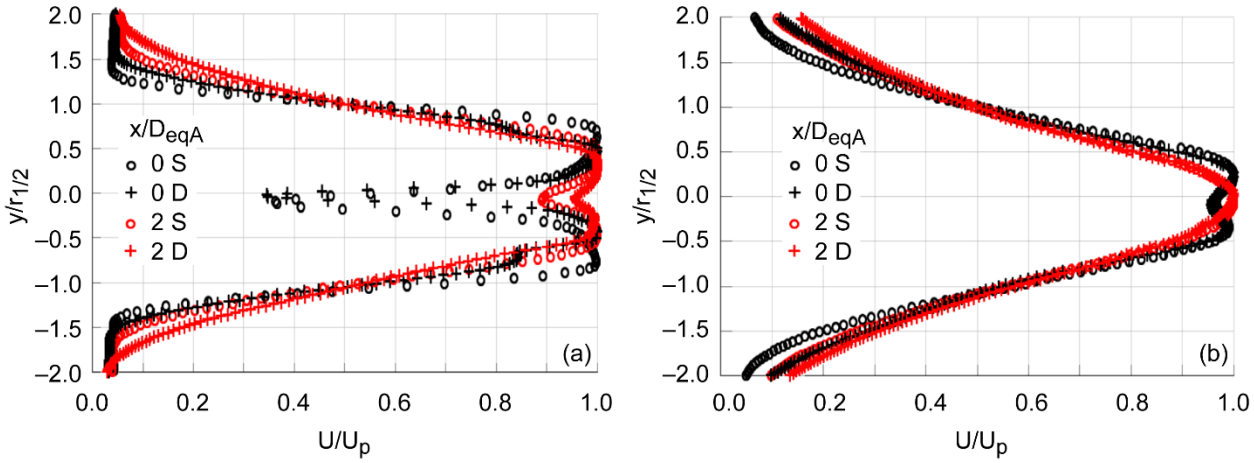

Figure 16.—The velocity at the indicated cross-stream planes for the unheated single-stream (S) and dual-stream (D) jets. The data were acquired at $M_{fj} = 0.0$ with the $A_b/A_c = 1.0$ nozzle system.

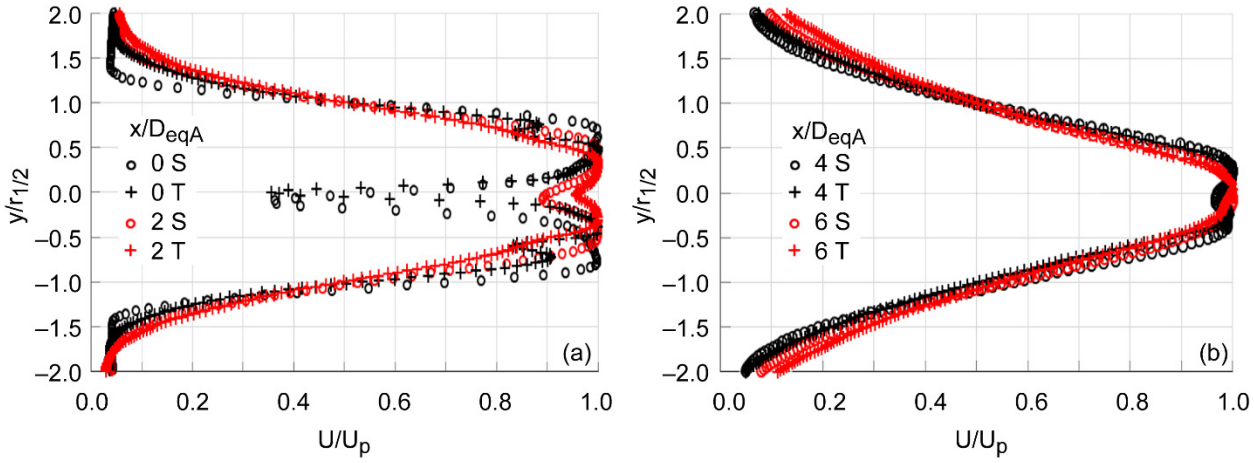

Figure 17.—The velocity at the indicated cross-stream planes for the unheated single-stream (S) and three-stream (T) jets. The data were acquired at $M_{fj} = 0.0$ with the $A_b/A_c = A_t/A_c = 1.0$ nozzle system.

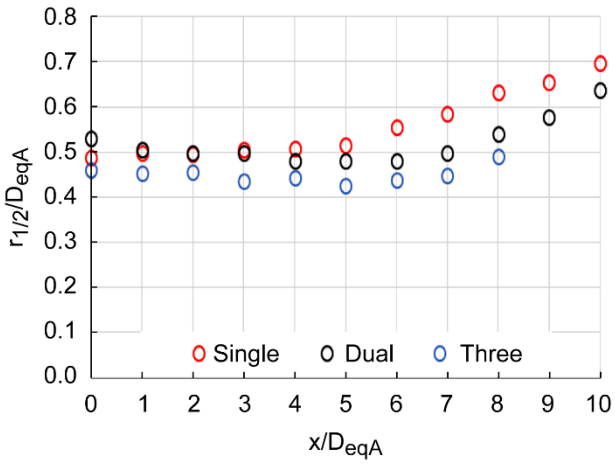

Figure 18.—The half-velocity radii for the unheated single-, dual-, and three-stream jets. The data were acquired with the $A_b/A_c = A_t/A_c = 1.0$ and for $M_{fj} = 0.0$.

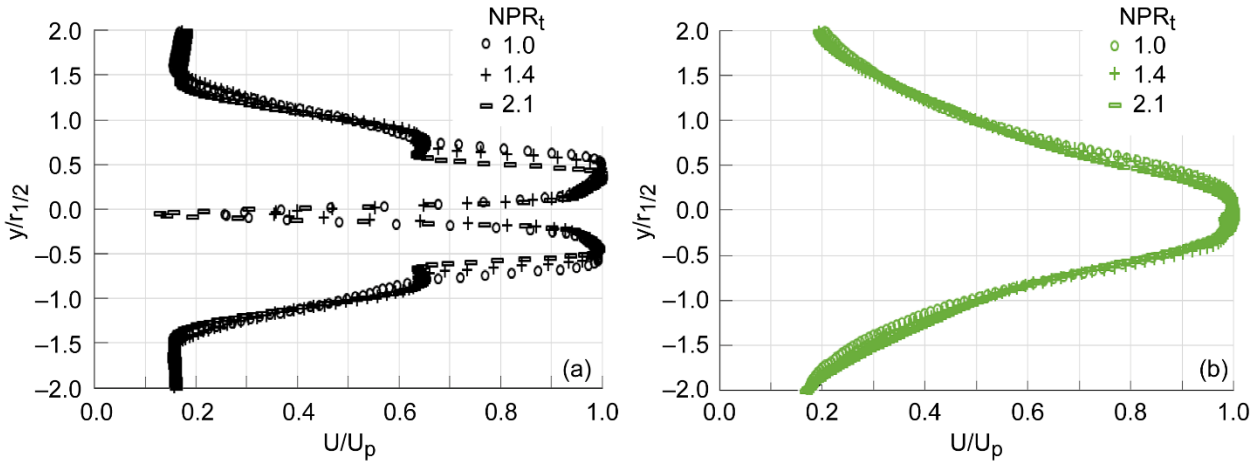

Figure 19.—The velocity for the heated jet conditions and $A_b/A_c = A_t/A_c = 1$. The black and green are for $x/D_{eqA} = 0$ and 4, respectively. The data are for $M_{fj} = 0.3$.

A plot of the normalized half-velocity radii ($r_{1/2}$) for the unheated single-, dual-, and three-stream jets is shown in Figure 18. The data were acquired for the nozzle areas used in Figures 16 and 17. For $x/D_{eqA} \geq 4$, the half-velocity radius decreases with increasing numbers of annular jet streams.

The cross-stream velocity profiles for the heated dual- and three-stream jets and $A_b/A_c = A_t/A_c = 1.0$ are shown in Figure 19. The data were acquired at $M_{fj} = 0.3$. Near the plug tip ($x/D_{eqA} = 0$), increasing the tertiary stream from $NPR_t = 1.4$ to 2.1 reduces the effective core-flow diameter. By $x/D_{eqA} = 4.0$, the normalized velocity profiles for the dual- and three-stream jets are the same and the introduction of the tertiary stream appears to have no impact on the further development of the normalized mean velocity profiles with downstream distance. The corresponding half-velocity radii are shown in Figure 20. The normalized half-velocity radii are similar for the dual-stream jet and the three-stream jet with $NPR_t = 2.1$. The three-stream jet with $NPR_t = 1.4$ has the lowest normalized half-velocity radii in Figure 20 for all axial stations. The mean velocities as a function of $(y-y_{1/2})/x$ are shown in Figure 21. For each tertiary condition, the velocity profiles at different cross-stream planes were nearly identical for $x/D_{eqA} > 4$ in the cross-plane region where $(y-y_{1/2})/x$ was linearly related to U/U_e. Additionally, as shown in Figure 21, the velocity profiles were identical for $NPR_t = 1.0$ and 2.1 in the cross-stream region where $(y-y_{1/2})/x$ was linearly related to U/U_e.

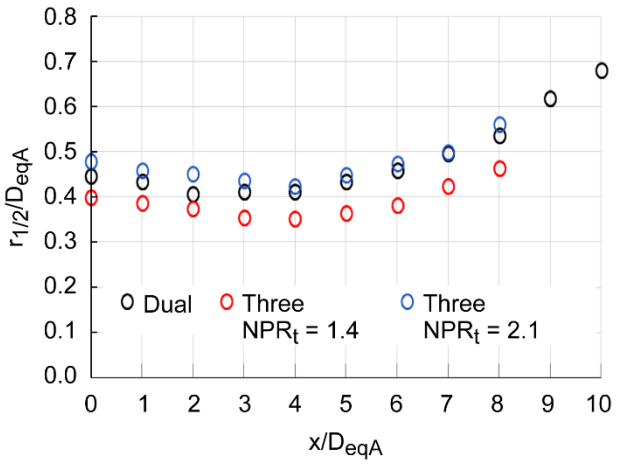

Figure 20.—The half-velocity radii for the heated single-, dual-, and three-stream jets. The data were acquired for M_{fj} = 0.3 with the A_b/A_c = A_t/A_c = 1.0 nozzle system.

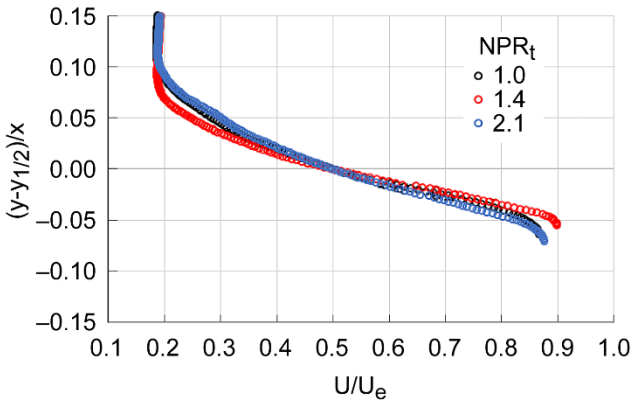

Figure 21.—The velocity at the indicated cross-stream planes for the heated dual- and three-stream jets. The data were acquired for M_{fj} = 0.0 and with the A_b/A_c = A_t/A_c = 1.0 nozzle system.

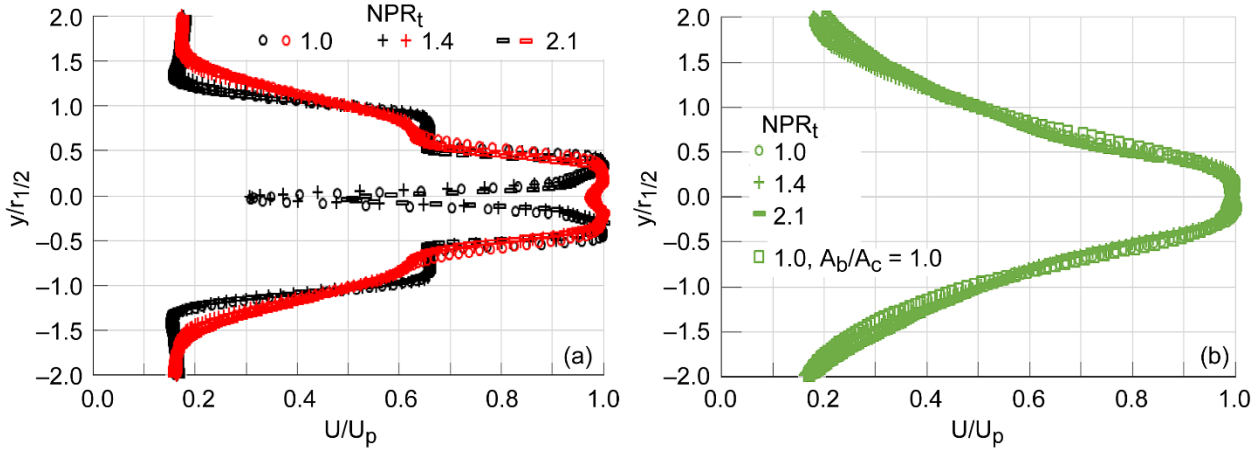

Figure 22.—The velocity for the heated dual- and three-stream jets. Unless otherwise indicated, the data are for A_b/A_c = 2.5. Black, red, and green symbols indicate x/D_{eqA} = 0, 2 and 4, respectively. The data are for M_{fj} = 0.3.

The impact of adding the tertiary stream on the resulting mean velocity for the large bypass-ratio nozzle system is shown in Figure 22. Unless otherwise indicated, the data are for A_b/A_c = 2.5. All data were acquired with A_t/A_c = 1.0, M_{fj} = 0.3, and heated jet conditions. The data in black, red, and green are for x/D_{eqA} = 0, 2, and 4, respectively. Near the nozzle tip (x/D_{eqA} = 0 and 2), the rapid increase in $y/r_{1/2}$ at U/U_p = 0.65 is far greater for the A_b/A_c = 2.5 than for the A_b/A_c = 1.0 (Fig. 19) and is entirely associated with the bypass stream as there is no observable impact on the velocity profiles with the addition of the tertiary stream. By x/D_{eqA} = 4, the velocity profiles associated with the A_b/A_c = 2.5 for all tertiary conditions are the same as the dual-stream jet for the A_b/A_c = 1.0 nozzle. The half-velocity radii for the dual stream jet at the two bypass-to-core area ratios are shown in Figure 23. The half-velocity radii are similar for all normalized cross-stream planes.

The velocity profiles near the plug tip (x/D_{eqA} = 0) produced by the A_b/A_c = 1.0 and A_t/A_c = 0.6 nozzle system are shown in Figure 24. The results are similar to those in Figure 19 although the addition of the tertiary stream at NPR_t = 2.1 has a slightly greater impact on the resulting mean velocity for A_t/A_b = 1.0 than for A_t/A_c = 0.6.

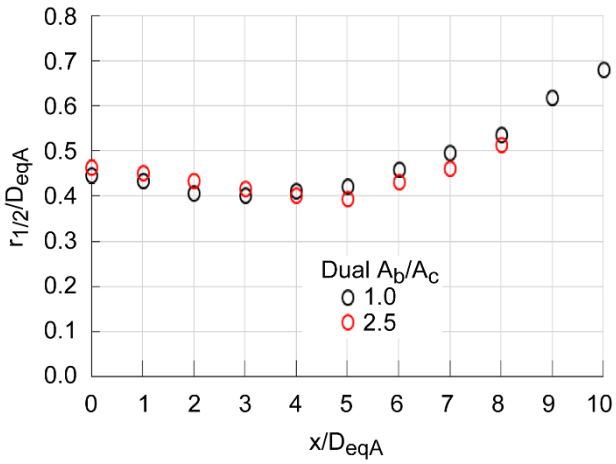

Figure 23.—The half-velocity radii for the heated jet conditions and the indicated dual-stream jets. The data were acquired with the A_t/A_c = 1.0 and M_{fj} = 0.3.

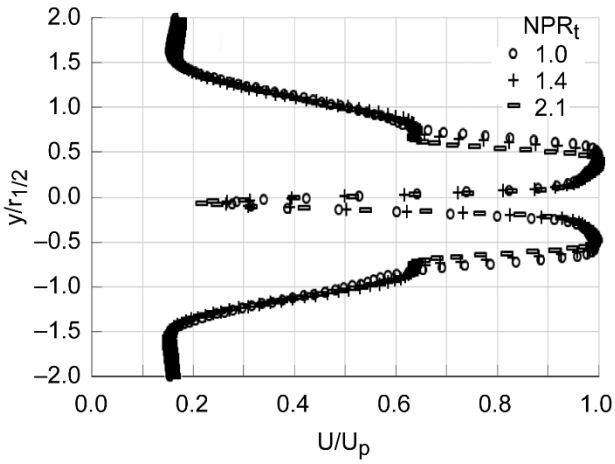

Figure 24.—The mean velocity for the heated dual- and three-stream jets at x/D_{eqA} = 0. The data were acquired with the A_b/A_c = 1.0 and A_t/A_c = 0.6 nozzle system and for M_{fj} = 0.3.

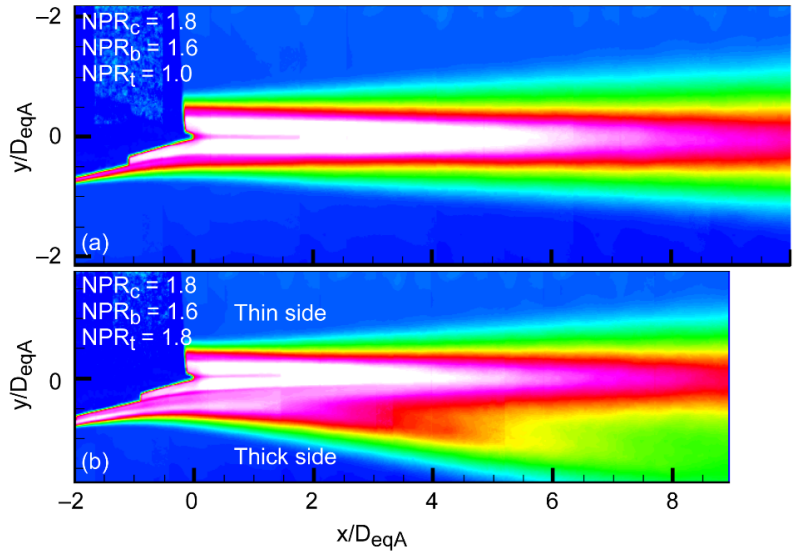

Figure 25.—The mean velocity in the center plane for the unheated dual-stream (top) and three-stream offset (bottom) jets. The conditions are indicated on the contour plots. The legend is the same as that in Figure 4 with U_e equal to the core exit velocity. The data were acquired for M_{fj} = 0.0.

The velocity in the center plane for the unheated dual- and three-stream jets using the offset tertiary duct are shown in Figure 25. The data were acquired for A_b/A_c = 1.0 and M_{fj} = 0.0. The introduction of the offset tertiary stream elongates the bypass potential core and increases the jet width on the "thick side" (lower side) of the jet for $x/D_{eqA} < 6$. The corresponding velocities in cross-stream planes for the offset three-stream jet are shown in Figure 26. The presence of the bypass potential core is identifiable for $0 \leq x/D_{eqA} \leq 2$ and a secondary velocity peak associated with the bypass flow persists on the "thick side" of the offset tertiary stream for all cross-stream planes investigated.

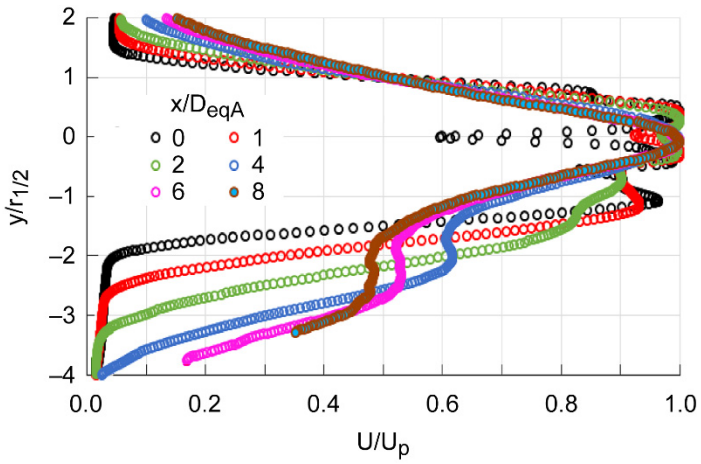

Figure 26.—The velocities at the indicated cross-stream plane for the unheated three-stream jet with the tertiary offset. The data are for NPR_t = 1.8 and M_{fj} = 0.0 and were acquired with the A_b/A_c = 1.0 nozzle system.

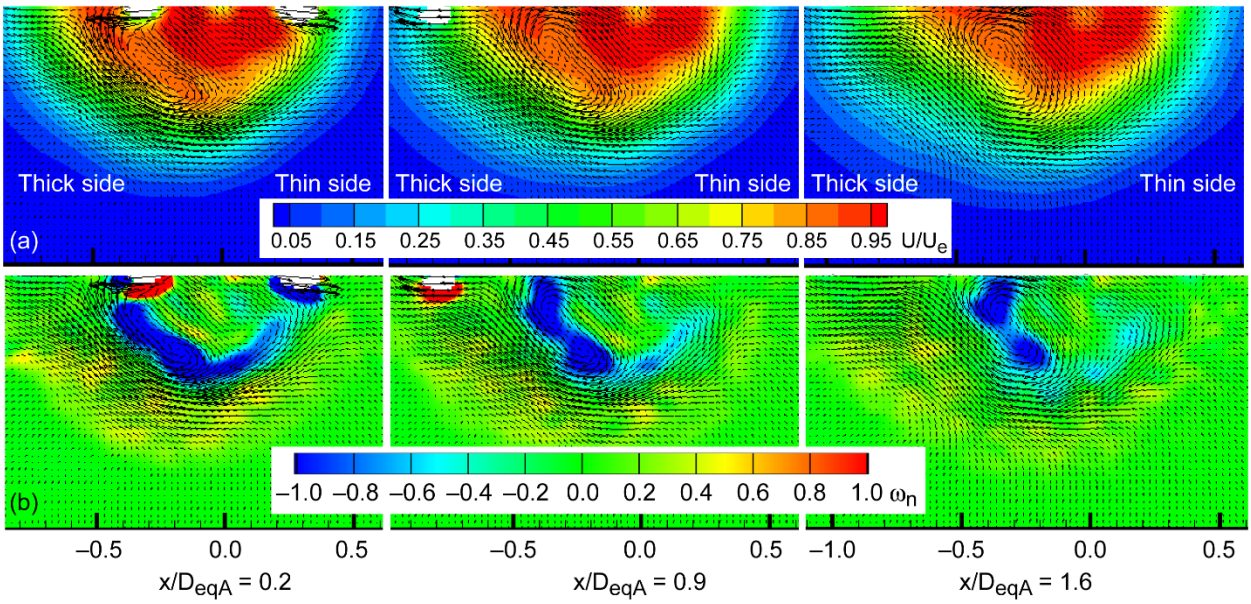

Figure 27.—The normalized mean axial velocity (top row) and normalized vorticity (bottom row) for the unheated three-stream offset jet with NPR_t = 1.8 for the indicated cross-stream planes. Also shown are the cross-stream velocity vectors. The data were acquired for M_{fj} = 0.0.

The axial velocity and normalized mean axial vorticity (ω_n) contours in cross-stream planes for the three-stream jet with the offset tertiary stream are shown in Figure 27. The data were obtained with the stereo PIV setup so only one half of the jet was captured. The "thick" and "thin" sides of the flow are on the left and right side of each plot, respectively. The vorticity has been normalized by the ratio of the core exit velocity and the equivalent diameter computed from the total nozzle exit area. Also shown in the Figure are cross-stream velocity vectors. The introduction of the offset tertiary stream produces axial vorticity in the shear layer between the core and bypass streams that persists for roughly two equivalent diameters downstream of the core plug tip. The vorticity distorts the core flow and impacts jet mixing.

B. Axial Turbulence Characteristics

The axial component of the turbulence intensity in the center plane for the unheated and heated single-stream jets is shown in Figure 28. The root-mean-square of the axial component of the velocity fluctuations is given by u'. While normalized peak values are roughly the same for the two jets, the turbulence intensity decays more rapidly downstream of the peak location for the hot jet than for the cold jet. The peak level occurs at an axial location near the end of the potential core for the cold jet and slightly downstream of the end of the potential core for the hot jet.

The turbulence intensities for the unheated single-stream jet in cross-stream planes between $0 \leq x/D_{eqA} \leq 8$ are shown in Figure 29. The cross-stream coordinate has been normalized by $r'_{1/2}$, the radial distance to the location where the turbulence intensity is half that of the peak level which radially aligns the outer turbulence intensity peak across all configurations (an alignment that was not possible using the more traditional vorticity thickness often used in single-stream jet comparisons). As will be shown, the use of $r'_{1/2}$ produced the best collapse of the data for the single-, dual-, and three-stream jets. It should be noted $r'_{1/2}$ is greater than $r_{1/2}$. Two major peaks occur at roughly $y/r'_{1/2} = 0.75$ and -0.75 and are associated with the shear layer between the core stream and ambient air. The smaller peak along the central region of the jet for $x/D_{eqA} \leq 4$ is associated with the plug wake. The peak turbulence intensity occurs around $x/D_{eqA} = 6$. The secondary peak associated with the plug wake is no longer evident in the cross-stream plots for $x/D_{eqA} \geq 6$.

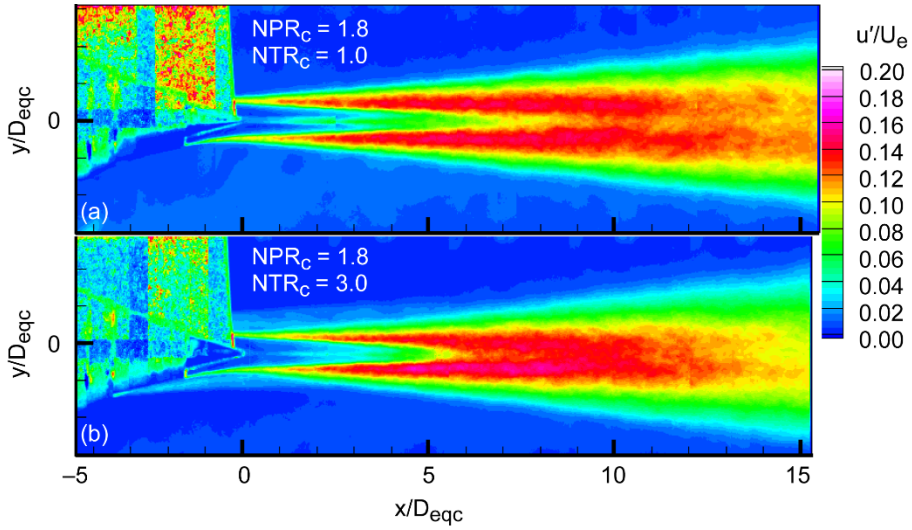

Figure 28.—The turbulence intensity for the unheated (top) and heated (bottom) single-stream jets. The data were acquired at $M_{fj} = 0.0$.

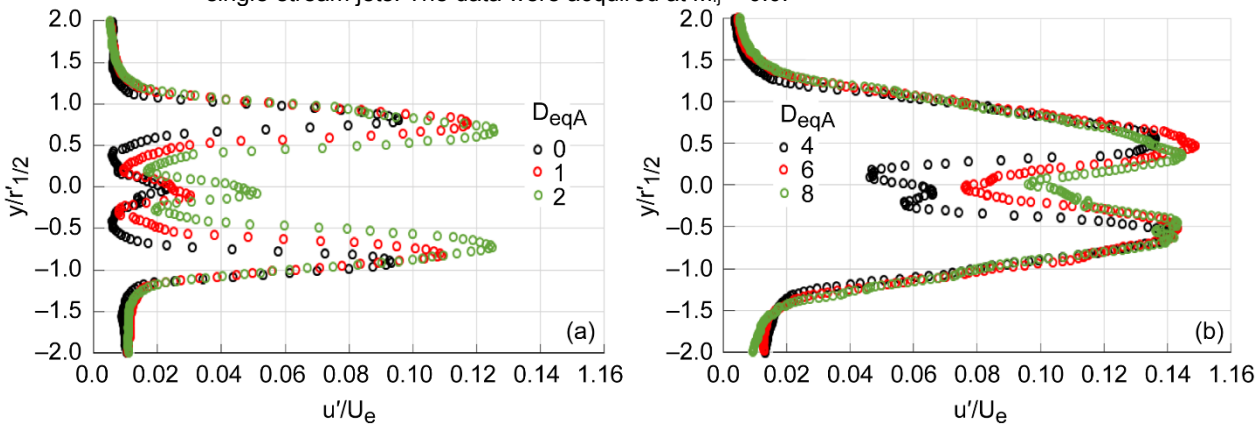

Figure 29.—The turbulence intensity at the indicated cross-stream planes for the unheated simulated single-stream jet with $A_b/A_c = 1.0$ and $M_{fj} = 0.0$.

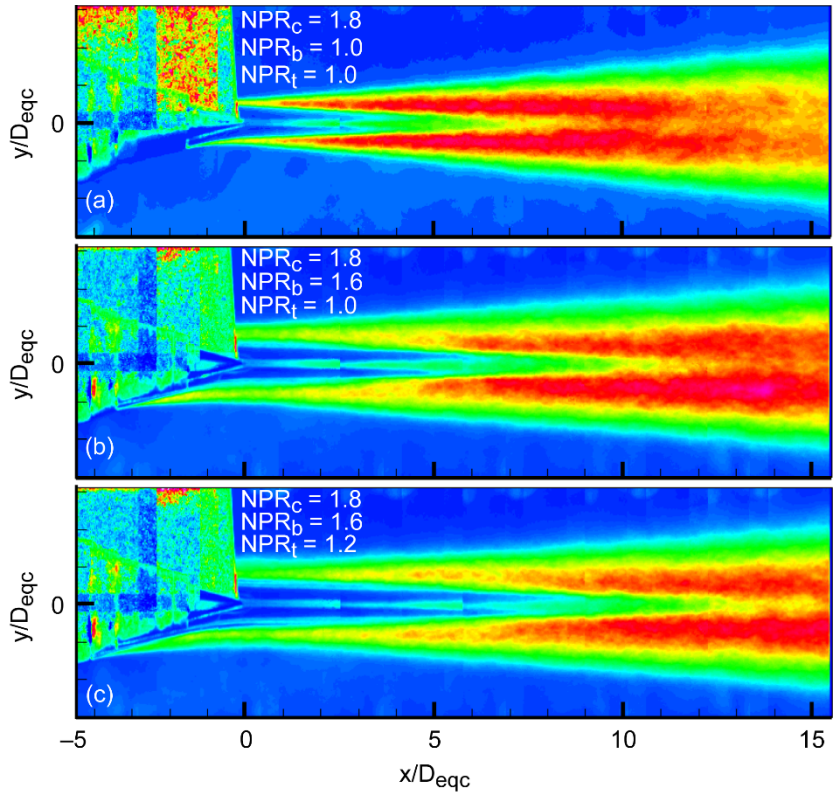

Figure 30.—The turbulence intensity in the center plane for the unheated single-, dual-, and three-stream jets. The jet conditions are indicated on the contour plots. The legend is the same as that in Figure 28 with U_e replaced by the mass weighted velocity at the nozzle exit. The data were acquired for $M_{fj} = 0.0$.

The turbulence intensities for the unheated single-, dual-, and three-stream jets are shown in Figure 30. With each added stream, the location of the peak turbulence intensity moves downstream. It should be noted that the location of the peak level for the three-stream jet may occur downstream of the last measurement station. The corresponding turbulence intensities in cross-stream planes are shown in Figure 31. For the dual- and three-stream jets, the mass-weighted velocity is used for U_e. For $x/D_{eqA} \leq 4$, two major turbulence intensity peaks occur at $y/r'_{1/2}$ roughly equal to ±0.75 which are associated with the shear layer between the jet and ambient air and a secondary peak occurs in the center of jet which is associated with the plug wake. The dual- and three-stream jets do not display additional turbulence intensity peaks for the shear layers between the annular and the interior jet streams. Near the plug tip ($x/D_{eqA} = 0$), peak normalized turbulence intensity levels are nearly the same of the single-, dual-, and three-stream jets. For intermediate axial stations ($2 \leq x/D_{eqA} \leq 4$), peak normalized turbulence intensity levels for the dual- and three-stream jets are nearly the same and lower than those for the single-stream jet. For axial stations near the end of the potential core ($6 \leq x/D_{eqA} \leq 8$), peak normalized turbulence intensity levels for the three-stream jet slightly exceed those for the single- and dual-stream jets. However, for all axial stations investigated, the differences in peak levels for the three jet configurations in Figure 31 were no greater than 10 percent of the highest normalized turbulence intensity levels and the slight differences at $6 \leq x/D_{eqA} \leq 8$ may have been associated with asymmetries in the flow-fields.

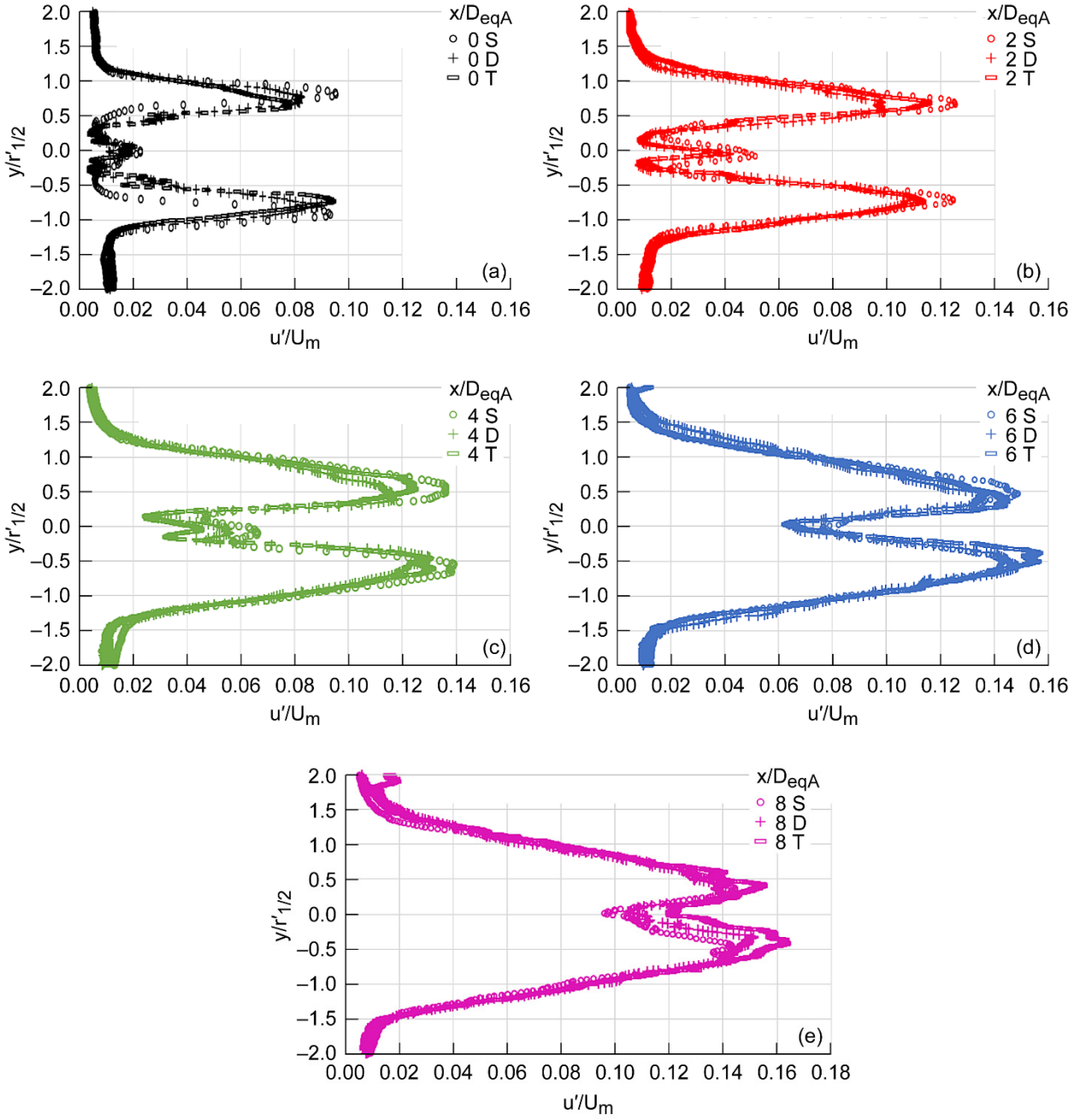

Figure 31.—The turbulence intensity for the unheated single-stream (S), dual-stream (D), and three-stream (T) jets. The data were acquired with Ab/Ac = At/Ac = 1 and at Mfj = 0.0. Black, red, green, blue, and magenta indicate x/DeqA = 0, x/DeqA = 2, x/DeqA = 4, x/DeqA =6, x/DeqA = 8.

The impact of increasing the velocity of the tertiary stream on the turbulence intensities of the heated jets is shown in Figure 32 for $A_b/A_c = A_t/A_c = 1$. Four major peaks (two on each side of the jet centerline) occur in the turbulence-intensity profiles for $0 \le x/DeqA \le 2$. These peaks are associated with the shear layers between the core and bypass streams and between the combined bypass-tertiary stream and the simulated flight stream. As shown in the contour plot of Figure 33, the tertiary stream has mixed with the bypass flow and simulated flight stream well upstream of the plug tip. At $x/D_{eqA} = 0$, the highest normalized turbulence intensity level is associated with the $NPR_t = 2.1$ tertiary condition and similar turbulence intensity levels (but lower than that for $NPR_t = 2.1$) occur for the $NPR_t = 1.0$ and 1.4 tertiary conditions. Asymmetries occur for the dual-stream jet for $x/D_{eqA} \ge 2$ and for the three-stream jets for $x/D_{eqA} \ge 0$. Flow asymmetries have been noted in previous dual-stream jet experiments (Ref. 13) and investigated numerically by Birch et al. (Ref. 14). At $x/D_{eqA} = 2$, the highest turbulence intensity level is associated with the dual-stream jet which displays the largest asymmetries at this cross-stream location. For $6 \le x/DeqA \le 8$, the highest turbulence intensity levels occur for the three-stream jet with $NPR_t = 1.4$.

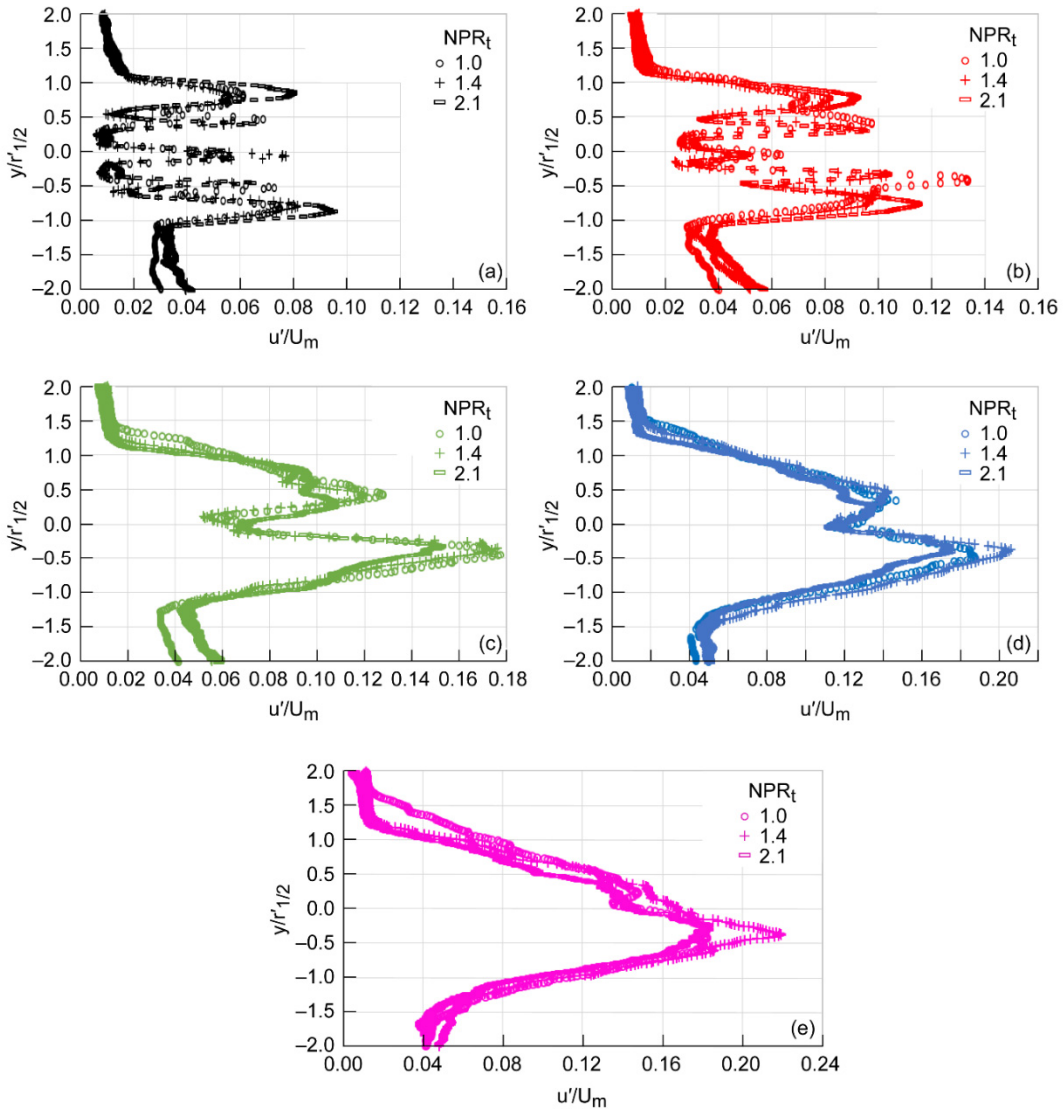

Figure 32.—The normalized turbulence intensity for the heated three-stream jets at the indicated NPR_t. The data were acquired with $A_b/A_c = 1$ and at $M_{fj} = 0.0$. Black, red, green, blue, and magenta indicate $x/D_{eqA} = 0$, $x/D_{eqA} = 2$, $x/D_{eqA} = 4$, $x/D_{eqA} = 6$, and $x/D_{eqA} = 8$, respectively.

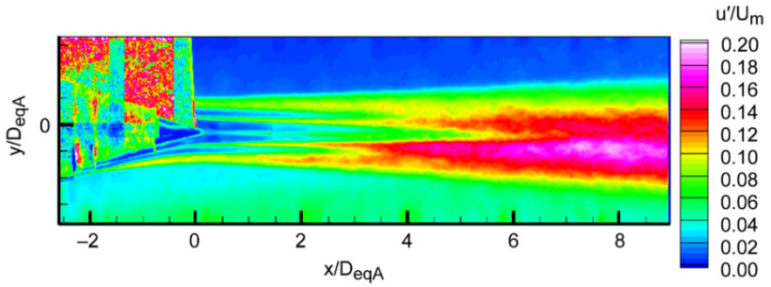

Figure 33.—The turbulence intensity in the center plane for the heated three-stream jet and NPR_t = 2.1. The data were acquired with A_b/A_c = 1 and M_{fj} = 0.3.

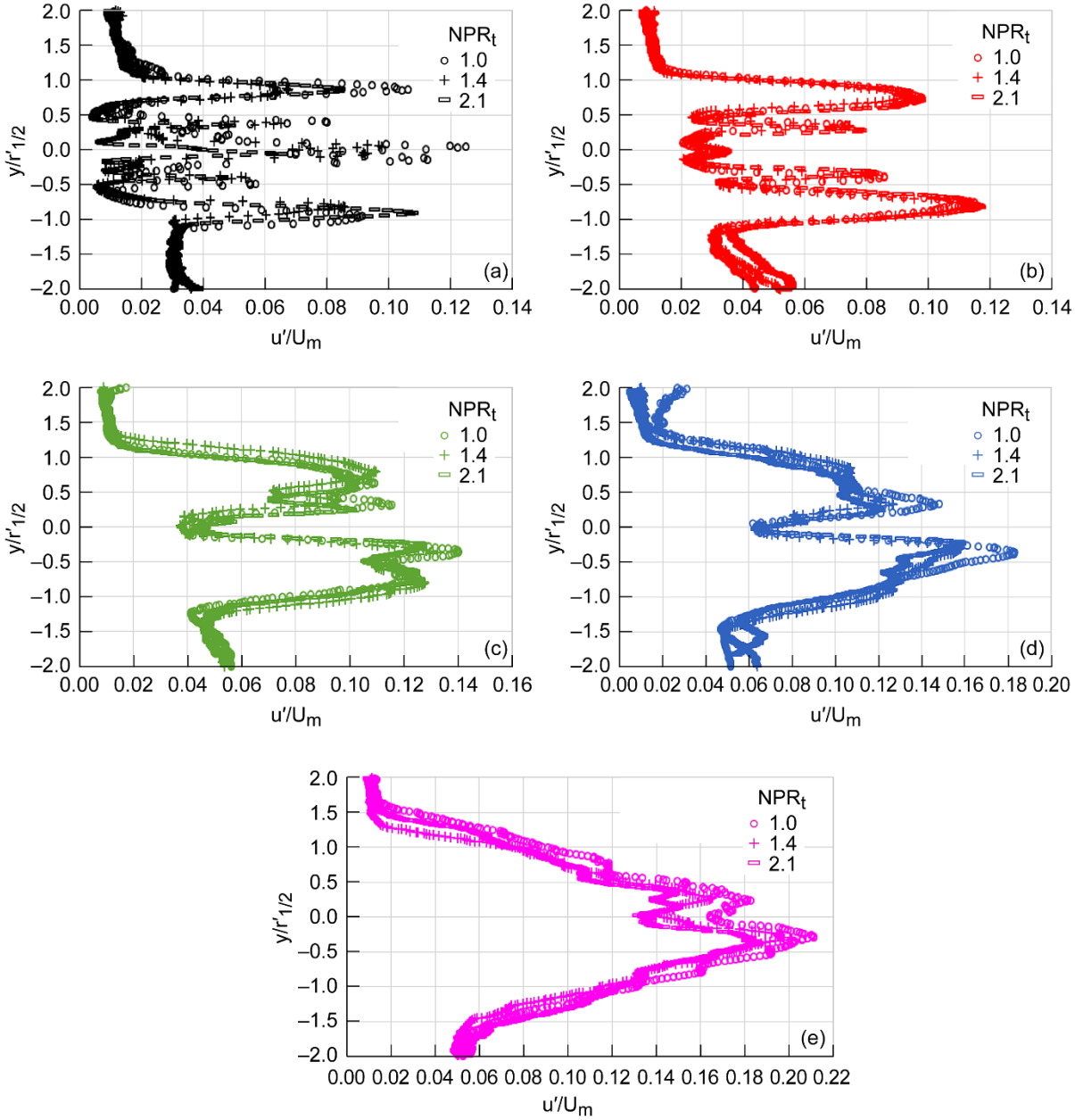

Figure 34.—The turbulence intensity for the heated three-stream jets at the indicated NPR_t. The data were acquired with A_b/A_c = 2.5 and at M_{fj} = 0.3. Black, red, green, blue, and magenta indicate x/D_{eqA} = 0, x/D_{eqA} = 2, x/D_{eqA} = 4, x/D_{eqA} = 5, and x/D_{eqA} = 7, respectively.

The impact of increasing the velocity of the tertiary stream on the turbulence intensity produced by the $A_b/A_c = 2.5$ and $A_t/A_c = 1.0$ nozzle system is shown in Figure 34 for $M_{fj} = 0.3$. Near the plug tip ($x/D_{eqA} = 0$), the normalized turbulence intensity levels for the dual-stream jet are higher than those for $A_b/A_c = 1.0$ (Fig. 32). For $2 \leq x/D_{eqA} \leq 4$, the dual- and three-stream jets have nearly identical normalized turbulence intensity levels and profiles. For axial stations near the end of the potential core ($5 \leq x/D_{eqA} \leq 7$), the dual-stream jet has the highest turbulence intensity levels.

A comparison of the turbulence intensity produced by the small and large bypass-to-core nozzles with $NPR_t = 1.4$ is shown in Figure 35 for heated jet conditions. For $x/D_{eqA} = 0$, the highest turbulence intensity levels occur for the large bypass-to-core nozzle system. For $2 \leq x/D_{eqA} \leq 5$, the small bypass-to-core nozzle system with significant flow asymmetries produces the highest turbulence intensities. For $x/D_{eqA} = 7$, the large bypass-to-core nozzle produces the highest normalized turbulence intensity.

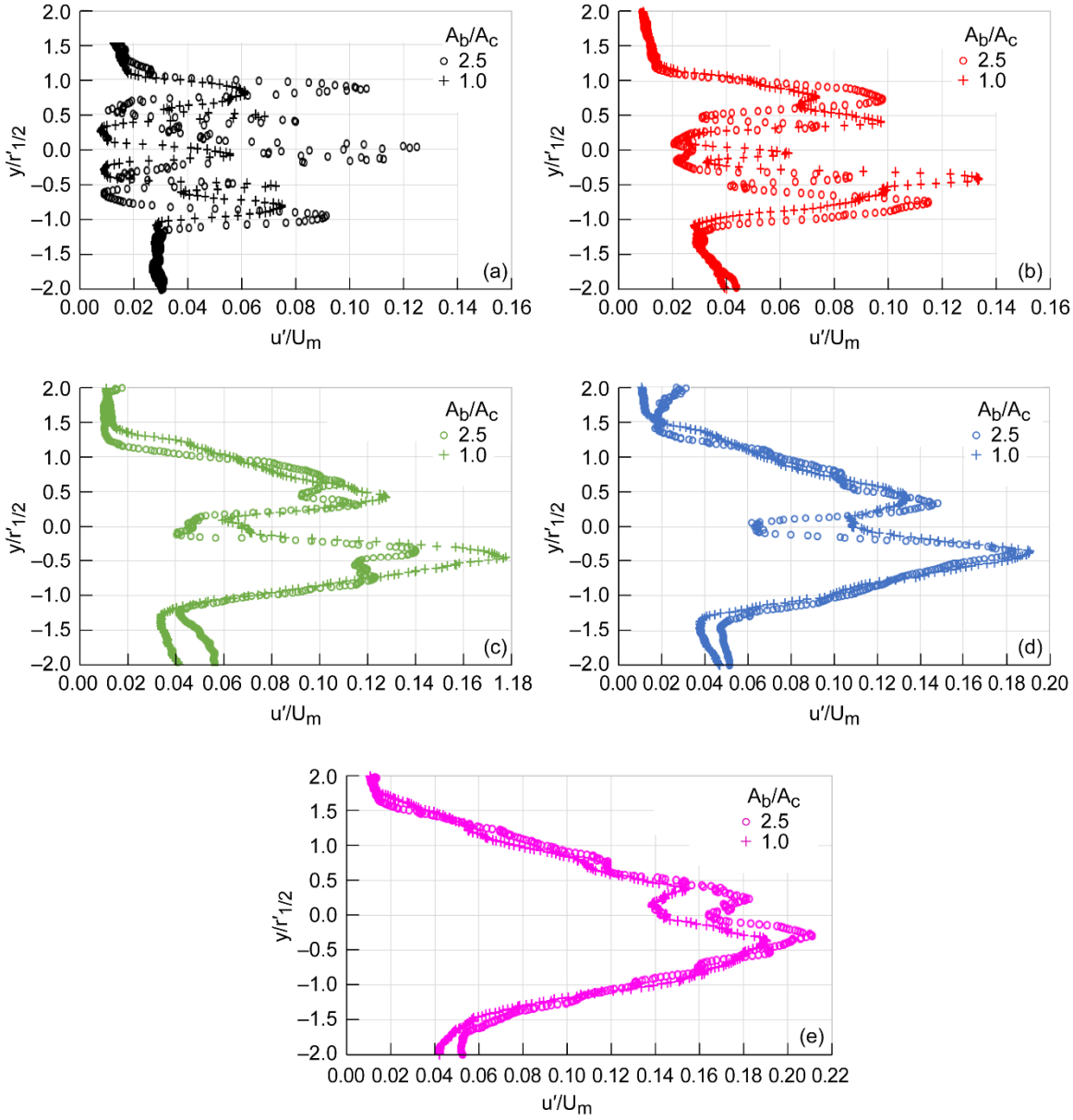

Figure 35.—The turbulence intensity for the heated three-stream jets with $NPR_t = 1.4$ and the indicated bypass-to-core area ratio. The data were acquired with $A_t/A_c = 1.0$ and at $M_{fj} = 0.3$. Black, red, green, blue, and magenta indicate $x/D_{eqA} = 0$, $x/D_{eqA} = 2$, $x/D_{eqA} = 4$, $x/D_{eqA} = 5$, and $x/D_{eqA} = 7$, respectively.

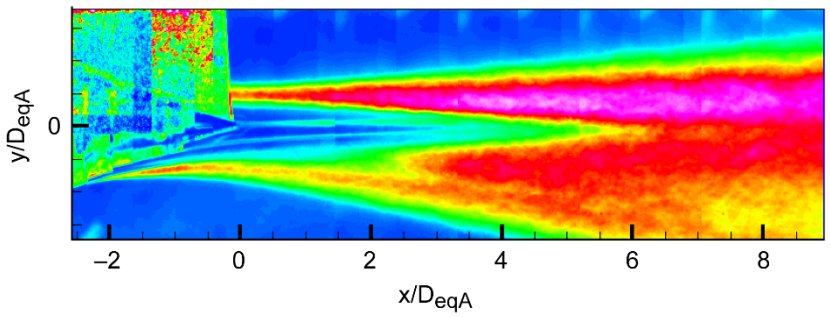

Figure 36.—The turbulence intensity in the center plane for the unheated offset three-stream jet with NPR_t = 1.8 and M_{fj} = 0.0. The legend is the same as that in Figure 31.

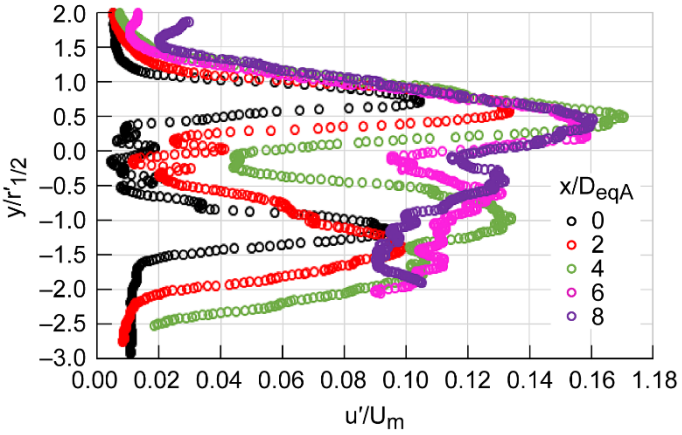

Figure 37.—The turbulence intensity in the indicated cross-stream planes for the unheated offset three-stream jet with NPR_t = 1.8 and M_{fj} = 0.0.

The turbulence intensity levels for the unheated offset three-stream jet with NPR_t = 1.8 are shown in the contour plot of Figure 36 and the cross-stream plot of Figure 37. The "thin" side of the jet is on the top side of each figure. As expected, the highest turbulence intensity levels occur on the "thin" side of the jet. The peak turbulence-intensity levels occur at roughly x/D_{eqA} = 4, well upstream of the peak turbulence intensity locations for all axisymmetric dual- and three-stream jets investigated. The peak normalized turbulence intensity levels on the "thick" side of the jet are below those for the axisymmetric dual and three-stream jets investigated.

IV. Conclusions

The three-stream jet investigation reported here used externally mixed, externally plugged, convergent nozzles with bypass-to-core area ratios equal to 1.0 and 2.5 and tertiary-to-core area ratios equal to 0.6 and 1.0. Comparisons were made with single-stream jets produced by operating only the core stream and dual-stream jets produced by operating the core and bypass streams. Both axisymmetric and offset tertiary streams were used in the three-stream jet experiments. Heated and unheated jet conditions were investigated for high-subsonic core-stream exhausts.

The axisymmetric jets were characterized by an outer shear layer between the outer jet stream and the ambient flow and a plug wake for axial stations near the plug tip. The plug wake persisted further downstream for the unheated jet than for the heated jet. For the heated jet conditions where the velocity differences between the core and bypass streams were greater than those for the unheated jets, an additional shear layer between the core and bypass flow was evident in the flow-field data. Similar

centerline velocity decay rates were obtained using the centerline velocity and the cross-stream velocity peak which occurred outboard of the jet centerline for axial locations upstream of the end the potential core. The normalized centerline velocities for the single-, dual-, and three-stream jets compared well when the axial distances downstream of the plug tip were normalized by the equivalent diameter based on the nozzle total exit area. The centerline velocity decay rates were reasonably approximated by a slightly modified version of Witze's (Ref. 7) equation (developed for single-stream jets) although the predicted potential core lengths were slightly longer than those measured with the discrepancy being greater for the unheated jet than the heated jet mostly likely due to the impact of the plug wake on jet mixing characteristics. The characteristic jet width as measured by the normalized radial location of the half-velocity peak ($r_{1/2}/D_{eqA}$) was slightly greater for the single-stream jet than for the dual- and three-stream jets near, and downstream of, the end of the potential core. The addition of the tertiary stream had a greater impact on the mean axial velocity for the small bypass-to-core area ratio nozzle system than for the large bypass-to-core area ratio nozzle system. Offsetting the tertiary stream introduced axial vorticity which distorted the core flow and impacted jet mixing.

The normalized axial turbulence intensities for the unheated single-, dual- and three-stream jets were similar although the single-stream jet had slightly higher levels than the dual- and three-stream jets for $2 \leq x/D_{eqA} \leq 4$ and the three-stream jet had the slightly higher levels than those for the single- and dual-stream jets for $6 \leq x/D_{eqA} \leq 8$. For the heated dual- and three-stream jets where the velocity difference between the bypass and core streams was greater than that for the unheated jets, additional peaks in the cross-stream plots of axial turbulence intensity occurred near the plug tip as a result of the shear layer between the core stream and the combined bypass and tertiary streams. These peaks were not present in the unheated data. For the same tertiary conditions, peak normalized turbulence-intensity levels were higher near the plug tip and near the end of the potential core ($x/D_{eqA} = 6$) for $A_b/A_c = 2.5$ than for $A_b/A_c = 1$. Offsetting the tertiary stream produced significantly higher axial turbulence intensity on the "thin" side of the jet relative to levels on the "thick" side of the jet. Peak levels occurred further upstream for the offset stream than for any of the axisymmetric jets investigated.

References

1. Henderson, B., "Aeroacoustics of Three-Stream Jets," AIAA–2012–2159, 2012.
2. Henderson, B., Leib, S., Wernet, M., "Measurements and Predictions of the Noise From Three-Stream Jets," AIAA–2015–3120.
3. Huff, D., Henderson, B., Berton, J., Seidel, J. "Perceived Noise Analysis for Offset Jets Applied to Commercial Supersonic Aircraft," submitted for publication at AIAA Science and Technology Forum and Exposition (SciTech 2016), 2016.
4. Dosanjh, D.S., "Flow and Noise Characteristics of Multi-Stream Supersonic Jets," AIAA-81-1977, 1981.
5. Papamoschou, D., Johnson, A., and Phong, V., "Aeroacoustics of Three-Stream High-Speed Jets From Coaxial and Asymmetric Nozzles," AIAA–2013–007, 2013.
6. Laurence, J., "Intensity, Scale, and Spectra of Turbulence in Mixing Region of Free Subsonic Jet," NACA Report 1292, 1956.
7. Witze, P., "Centerline Velocity Decay of Compressible Free Jets," AIAA J., vol. 12 [4], pp. 417–418, 1974.
8. Birch, S.F, and Eggers, J.M., *Free Turbulent Shear Flows*, NASA SP 321, vol. 1, pp. 11–40, 1972.
9. Lau, J.C., Morris, P.J. and Fisher, M.J., "Measurements in Subsonic and Supersonic Free Jets Using a Laser Velocimeter," J. Fluid Mech., vol. 93, part 1, pp. 1–27, 1979.
10. Bridges, J., and Wernet, M., "Establishing Consensus Turbulence Statistics for Hot Subsonic Jets," AIAA–2010–3751, 2010.
11. Yoder, D., Debonis, J., Georgiadis, N., Modeling of Turbulent Free Shear Flows, AIAA–2013–2721, 2013.

12. Bridges, J., and Wernet, M., “Turbulence Measurements of Separate Flow Nozzles With Mixing Enhancement Features,” AIAA–2002–2484, 2004.
13. Doty, M., Henderson, B., and Kinzie, K., “Turbulence Measurements of Separate Flow Nozzles With Pylon Interaction Using Particle Image Velocimetry,” AIAA J., vol. 45 [6], pp. 1281–1289, 2007.
14. Birch, S.F., Lyubimov, D.A., Secundov, A.N., and Yakubovsky, K.Y., “Numerical Modeling Requirements for Coaxial and Chevron Nozzle Flows, AIAA–2003–3287, 2003.
15. Murakami, E., Papmoschou, D., “Mean Flow Development in Dual-Stream Compressible Jets,” AIAA J., vol. 40 [6], pp. 1131–1138, 2002.
16. Soeder, R.H., Wnuk, S.P., and Loew, R. “Aero-Acoustic Propulsion Laboratory Nozzle Acoustic Test Rig User Manual,” NASA/TM—2006-212939, 2006.
17. Wernet, J.H. and Wernet, M.P., “Stabilized Alumina/Ethanol Colloidal Dispersion for Seeding High Temperature Air Flows,” Proceedings of the ASME Symposium on Laser Anemometry: Advances and Applications, Lake Tahoe, NV, 1994.
18. Gui, L., Werely, S.T., “A Correlation-Based Continuous Window-Shift Technique to Reduce The Peak-Locking Effect in Digital PIV Image Evaluation,” Experiments In Fluids, vol. 32, pp. 506–517, 2002.
19. Wernet, M.P., “Symmetric Phase Only Filtering: a New Paradigm for DPIV Data Processing,” *Measurement Science and Technology*, vol. 16, pp. 601–618, 2005.
20. Taylor, J.R., *An Introduction to Error Analysis*, University Science Books, Oxford University Press, Mill Valley, CA., pp. 142–144, 1982.